Nano Research

ISSN 1998-0124 CN 11-5974/O4
https://doi.org/10.1007/s12274-024-6665-7

Review Article

# Stable hydrogen-bonded organic frameworks and their photo- and electro-responses

Ying Hou[1,2], Xin-Song Huang[1], Sheng-Hao Gong[1,4], Chen Liu[1,4], Yangyang Liu[3] (✉), and Tian-Fu Liu[1,2] (✉)

[1] *State Key Laboratory of Structural Chemistry, Fujian Institute of Research on the Structure of Matter, Chinese Academy of Sciences, Fuzhou 350002, China*
[2] *University of Chinese Academy of Sciences, Beijing 100049, China*
[3] *Department of Chemistry and Biochemistry, California State University, Los Angeles, California 90032, USA*
[4] *College of Chemistry and Materials Science, Fujian Normal University, Fuzhou 350007, China*



**Received:** 28 February 2024 / **Revised:** 26 March 2024 / **Accepted:** 27 March 2024

## ABSTRACT

Hydrogen-bonded organic frameworks (HOFs) are a recent class of porous materials that have garnered considerable research interest owing to their distinctive characteristics. HOFs can be constructed through judicious selection of H-bonding motifs, which are further enforced by other weak intermolecular interactions such as π–π stacking, van der Waals forces, and framework interpenetration. Taking advantage of these interactions, we can expand the functional field of HOFs by introducing active molecules. Recently, researchers have made substantial advancements in using HOFs for chemical sensing, catalysis, proton conduction, biological applications, and others. The low bonding energy of H-bonds allows for precise control over the concentration of ligands in solvents, forming diverse HOF structures. These varied structures offer significant advantages for producing HOFs with photo-responsive and electro-responsive properties. However, the presence of H-bonds in HOFs results in their inherent lower stability compared to metal-organic frameworks (MOFs) and covalent-organic frameworks (COFs) formed via coordination and covalent bonds, respectively. As a result, the pursuit of stable and innovative HOF materials with novel functional sites remains an ongoing challenge. This review provides an overview of recent research progress in the development of new strategies for stable HOF synthesis and applications of HOFs with stimuli-responsive properties. We first classified all synthetic methods reported to date and discussed the stable HOFs synthesized, as well as their unique properties and applications. In addition, we summarized the applications of HOFs utilizing their synergistic responses to external stimuli, including photo, electrical, pressure, and chemical stimuli. We systematically reviewed stable HOF synthesis and applications, which may lead to a deeper understanding of the structure–activity relationship for these materials and guide future HOF design.

## KEYWORDS

stable hydrogen-bonded organic frameworks (HOFs), photo-response, electro-response, photoelectric synergistic response

## 1 Introduction

Molecular self-assembly is prevalent, such as the formation of the double helix structure in deoxyribonucleic acid (DNA) strands, the folding of tertiary structures in ribonucleic acid (RNA) strands, the formation of functional proteins from amino acids, and the construction of micelles from lipid molecules in the aqueous phase. Inspired by the intricate self-assembly processes observed in nature, self-assembly strategies have played a crucial role in chemistry, physics, biology, and materials engineering. It has emerged as a vital "bottom-up" approach for synthesizing new materials. Diverse assembly strategies enable the creation of a wide range of structures suitable for various applications. The DNA structure can be regarded as the cross-linking product that connects DNA components with increasing levels of complexity [1–4]. The construction of hydrogen-bonded organic frameworks (HOFs) shares similarities with protein structure assembly (Fig. 1(a)), where one-dimensional (1D) isomolecular chains are commonly built through hydrogen bonding interactions between building blocks. These molecular chains are assembled using π–π interactions to create porous framework materials. Moreover, the forces inside and outside the molecular chains can be adjusted. For instance, we synthesized the first porous polymer-based HOF (PHOF-1) by creating a one-dimensional molecular chain through covalent bonding and assembling the chain using hydrogen bonding (Fig. 1(b)) [5]. Various HOFs can be constructed using strategies to meet specific application requirements.

Unlike how units are connected in metal-organic frameworks (MOFs) and covalent-organic frameworks (COFs), HOFs are composed of organic units, including pure organic molecules and metal-containing organic molecules, which are synergistically regulated by H-bonding interactions and other interaction forces (e.g., π–π interactions, etc.) [6–15]. The development of HOFs progressed at a slower pace than that of MOFs in the subsequent decades due to the challenge of their poor stability [16–23]. In 2010, Chen et al. reported a microporous HOF with permanent porosity, denoted as HOF-1 [24], which marked a significant

Address correspondence to Yangyang Liu, yliu114@calstatela.edu; Tian-Fu Liu, tfliu@fjirsm.ac.cn

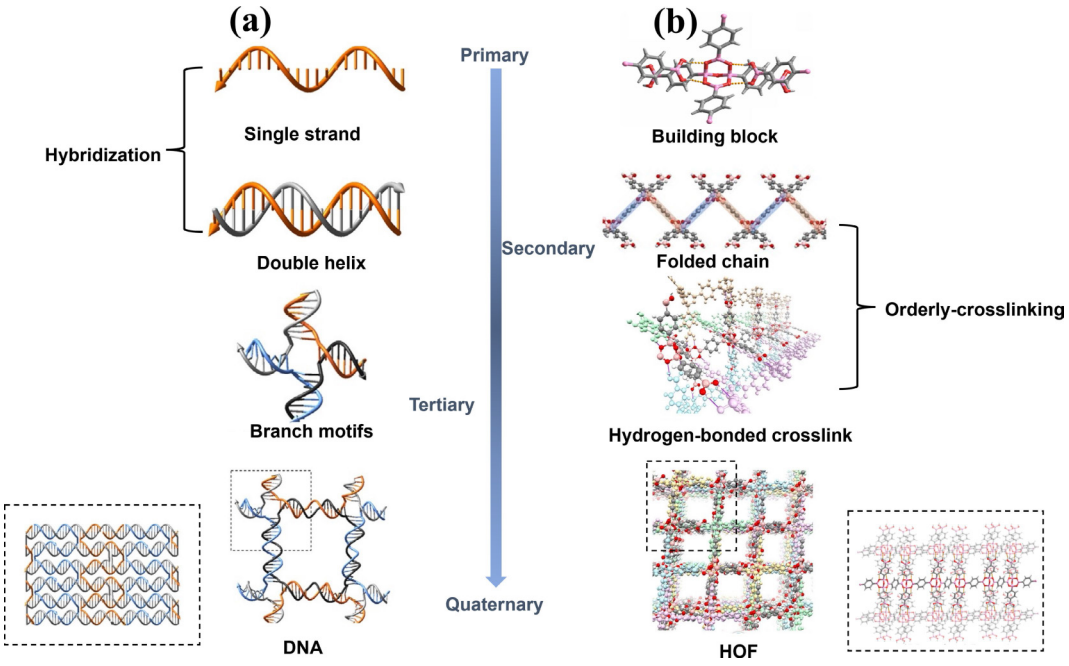


**Figure 1** The four levels of structural hierarchy in (a) DNA self-assembly, reproduced with permission from Refs. [1–4], © Wiley-VCH Verlag GmbH & Co. KGaA, Weinheim 2006, 2016, and 2018, respectively, and Hu, Y. Q. et al. 2020; and (b) HOF self-assembly, reproduced with permission from Ref. [5], © Liu, B. T. et al. 2023.

milestone in establishing the concept of permanent porosity in HOFs. Subsequently, this achievement sparked a renewed interest in HOFs, propelling extensive investigations into their diverse applications. HOFs offer greater accessibility in preparation compared to MOFs. The framework of HOFs relies on H-bonding forces, enabling the H nodes within the framework to recover through interactions with $H^+$ in water or various solvents, including hydrochloric acid (e.g., the hydrogen bond re-association mechanism for acid-assisted crystallization redemption (AACR)) (Fig. 2(a)) [25]. This characteristic of HOFs facilitates their recycling. Importantly, due to the absence of heavy metals in its synthesis, HOFs present a more promising outlook for biological applications than MOFs and other porous materials. HOFs also require mild synthesis conditions and have excellent solution processability (Fig. 2(b)). Currently, HOFs have shown great promise in various fields, including gas storage/separation [26–35], photocatalysis, chemical sensing, proton conduction, and biological applications. However, the stability of HOFs is still a concern due to the limitation of H-bonding. Despite the discovery of numerous HOFs, most fail to maintain structural integrity upon removing the guest molecules, leading to collapse. Therefore, enhancing the stability of HOFs is an urgent need.

This review focuses on recent advancements in HOFs, specifically in their photo-response, electro-response, and photovoltaic synergistic response. It also discusses existing strategies to enhance the stability of hydrogen-bonded organic frameworks.

## 2 Study on the construction of HOFs and their stability

### 2.1 Diverse H-bonding motifs for the construction of porous HOFs

HOFs are constructed similarly to MOFs and COFs, but with the distinction that HOFs utilize hydrogen bonds as the driving force for donor–receptor linkage. Typically, the structural units comprising the HOFs possess rigid characteristics that limit the free rotation and vibration of the construction pattern. The bonded by hydrogen bonds is attached to the rigid skeleton through a well-designed synthetic route. Subsequently, these binding sites self-assemble with adjacent components, completing the construction of HOFs through hydrogen bond interactions. Researchers are interested in the porosity of porous materials, which can be enhanced by controlling the bond length and employing bonding interactions based on orbital hybridization, such as $sp^2$ hybridization and $sp^3$ hybridization. The structural stability of HOFs can be improved by incorporating electrostatic forces, π–π interactions, and introducing multiple hydrogen bonds within the frameworks. However, increasing the number of bonds can also diminish the porosity; thus, balancing the stability and porosity of HOFs requires careful design and optimization. To address the balance between stability and permanent porosity in HOFs, researchers have explored various approaches to constructing porous HOFs using different motifs.

Initially, the diaminotriazines (DAT) moiety emerged as a well-known synthon for researchers due to its possession of multiple hydrogen bonding sites (Fig. 3). Two-dimensional (2D) or three-dimensional (3D) frameworks can be formed by attaching DAT molecules through hydrogen bonds. Furthermore, the interaction between two DATs can give rise to three distinct structural units, thereby increasing the diversity in DAT construction (Fig. 3(a)). Researchers have utilized these building blocks to fabricate a range of porous HOFs, including HOF-3 [36], HOF-4 [37], HOF-5 [38], HOF-6 [39], HOF-7 [40], HOF-9 [41], HOF-10 [42], and UPC-HOF-6 [43], etc. These HOFs have been studied for various applications and contributed significantly to the development of the field.

### 2.2 The classification of synthetic strategies for stable HOFs

To this date, various strategies have been employed to improve the stability of HOFs. We classified the methods reported in recent literature into primarily five strategies: (1) π–π stacking, (2) highly interpenetrated networks, (3) chemically cross-linked HOFs, (4) charge-assisted H-bonds, and (5) mechanical synthesis.

**π–π stacking.** The π–π stacking interaction is a force that arises between two or more aromatic rings. Introducing π–π stacking in HOFs enhances the stability of two-dimensional HOFs that contain conjugated systems. Through the appropriate design of

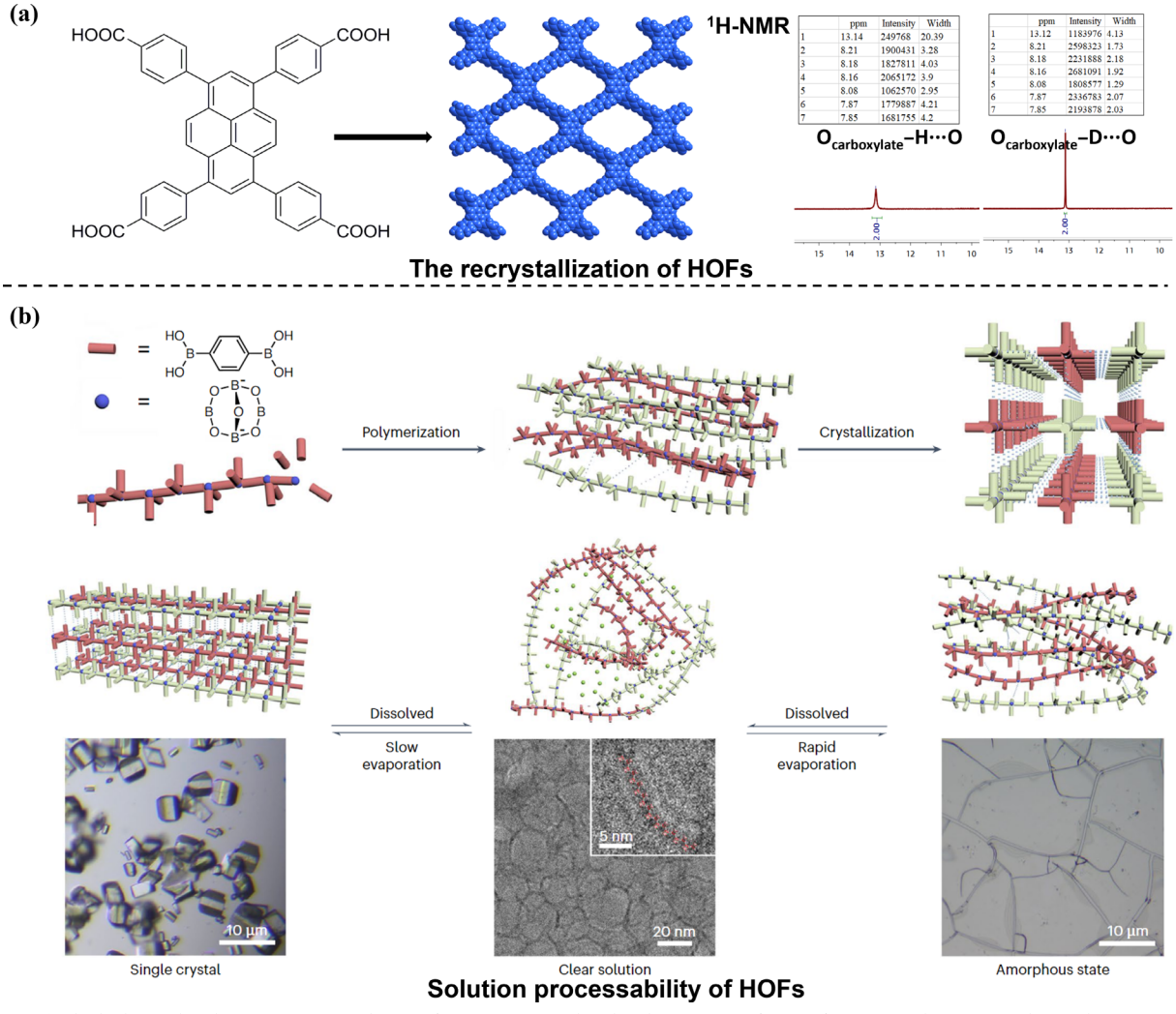


**Figure 2** (a) The hydrogen-bond re-association mechanism for AACR. Reproduced with permission from Ref. [25], © Wiley-VCH Verlag GmbH & Co. KGaA, Weinheim 2018. (b) The solution processability of HOFs. Reproduced with permission from Ref. [5], © Liu, B. T. et al. 2023.

the organic frameworks, these HOFs can also form three-dimensional frameworks with remarkable thermal stability and enhanced resistance to organic solvents as well as acidic and basic aqueous solutions, owing to the inert nature of the aromatic species. Miljanic and co-workers [44] have conducted an extensive investigation into the relationship between structure and porosity in porous molecular crystals. They synthesized over a dozen potential precursors for all-organic porous molecular crystals through a combination of Cu and Pd catalysis, inert atmosphere, and chemical and solvothermal synthesis. This series included variations in geometries, lengths, and the propensity for H-bonding and π–π stacking. Analysis of the crystal structures of the examined precursors revealed that both hydrogen bonding and π–π stacking capabilities are essential for the formation of porous structures.

Through careful observation of the crystal structures of SOF-7 [45] and HOF-TCBP [27] in 2018, it was discovered that the entire structure exhibited widespread and stable π–π interactions even after heating or water treatment. It demonstrated that selecting planar organic building blocks with substantial π-conjugated systems facilitates the formation of structures featuring extensive and robust π–π interactions, ultimately leading to stable frameworks. Considering HOFs can be designed at the molecular level, this strategy can be implemented through the choice of appropriate organic building blocks with extended π-conjugated systems. For example, $H_4$TBAPy, a planar molecule possessing a substantial π-conjugation system and four carboxylic acids, was selected as the building block for HOF construction. As expected, the resulting HOF, named PFC-1 (PFC = porous material from FJRSM, CAS), exhibited a high surface area of 2122 $m^2 \cdot g^{-1}$ and excellent chemical stability, which can withstand concentrated hydrochloric acid (12 M) for at least 117 days (Fig. 4) [25]. Strikingly, the thermal damage of PFC-1 can be easily remedied by AACR, which we have observed for the first time in HOFs.

Next, we sought to improve the stability of the frameworks using similar organic building blocks containing porphyrins. We hypothesized that altering the metal center of the porphyrin would result in a significant modification of the electronic structure of the macrocycles, the axial bonding/interactions, and the geometry of the peripheral substitutions. These changes can exert a substantial influence on the stability of HOFs [46]. To test this hypothesis, we incorporated various transition metal centers into porphyrins and synthesized HOFs possessing the same network topology. We found that the variation in metal centers in porphyrin led to significant changes in non-covalent interactions, orbital overlap, and molecular geometry, thus producing a series of metalloporphyrin HOFs with high surface area and excellent stability. For instance, the structure of one such HOF, PFC-73-Ni, was still intact after immersion in boiling water, concentrated hydrochloric acid, and heating to 270 °C.

**Highly interpenetrated networks.** The Interpenetrated network is a widely used approach to improve the stability of porous materials. The stability of HOFs can be effectively controlled by manipulating reactant concentrations, utilizing

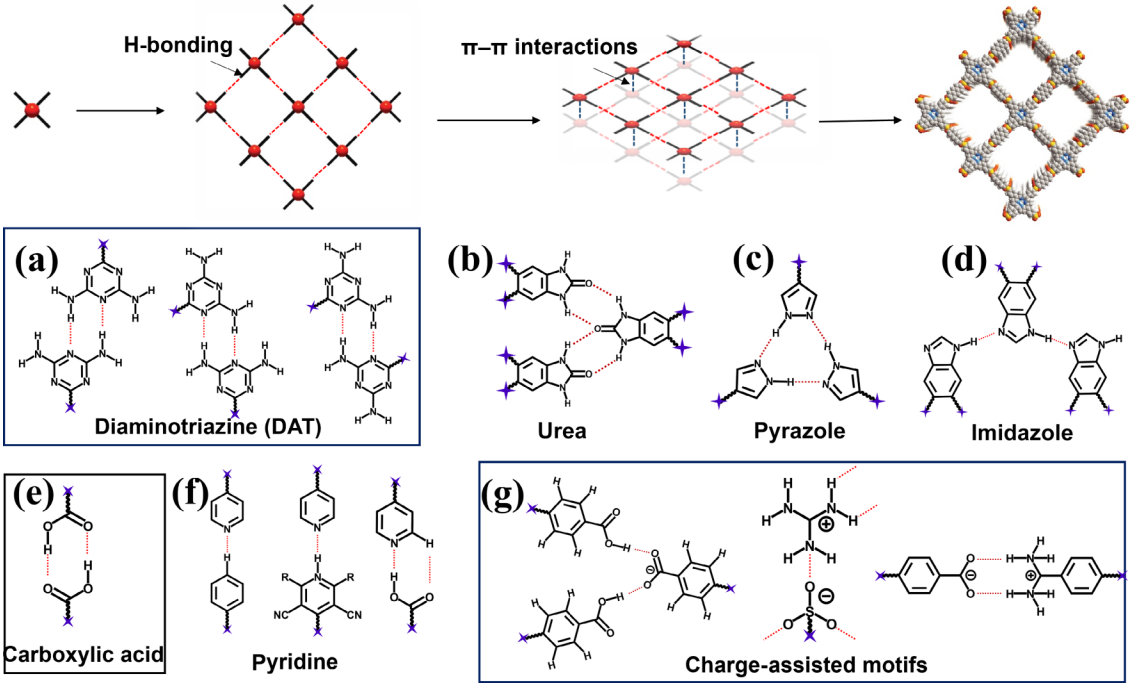


**Figure 3** H-bonding motifs used for the construction of porous HOFs.

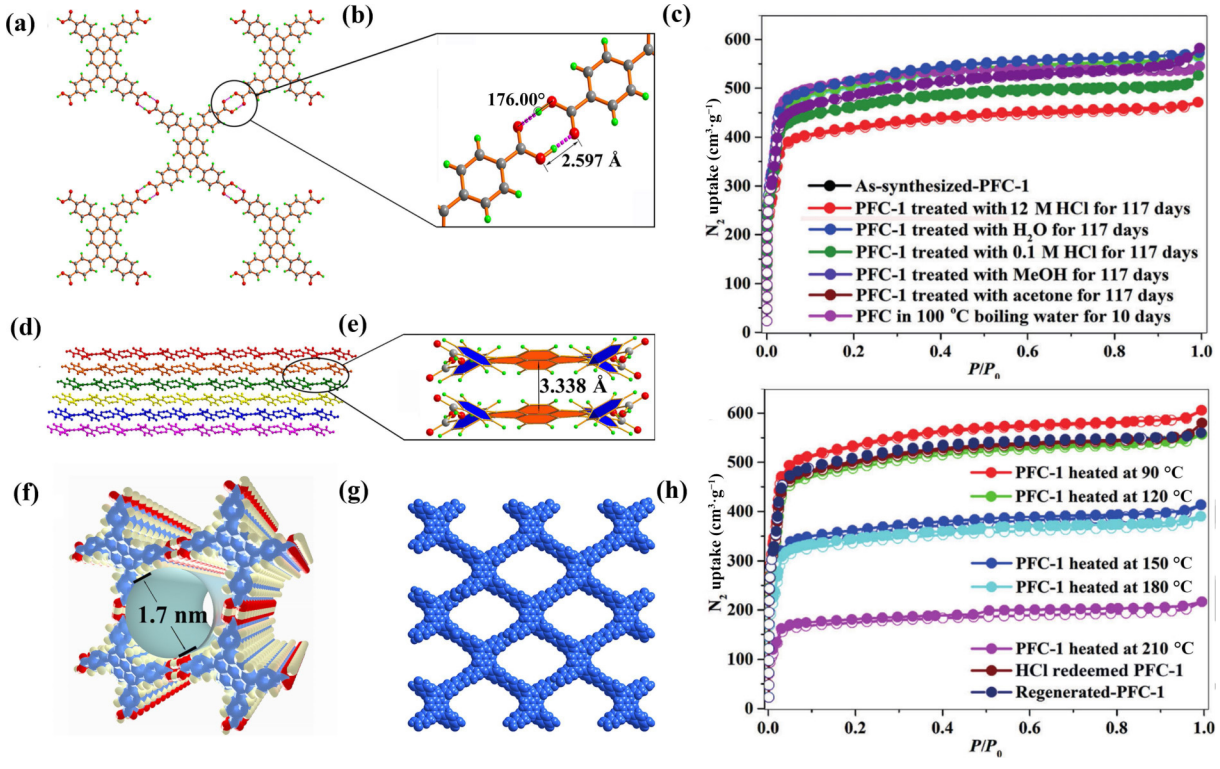


**Figure 4** (a) View of the structure of PFC-1 and the connection of adjacent building blocks. (b) Hydrogen-bond length and angle in PFC-1. (c) $N_2$ adsorption isotherms (77 K) of PFC-1 heated at different temperatures for 6 h, and the acid/solvent-treated PFC-1. (d) The stacking of 2D layers in PFC-1. (e) Face-to-face π–π interactions in PFC-1. (f) 1D channels in PFC-1. (g) Representation of the porous framework of PFC-1. (h) $N_2$ adsorption isotherms (77 K) of PFC-1 immersed in different solvents and heated at varying temperatures. Reproduced with permission from Ref. [25], © Wiley-VCH Verlag GmbH & Co. KGaA, Weinheim 2018.

templates, and epitaxial synthesis. Interpenetration is a crucial structural characteristic of HOFs that fulfills multiple functions: (1) enhancing the physical stability of the framework, (2) imparting flexibility and dynamic properties to the HOF structure, and (3) finely adjusting the pore environment. Additionally, it aids in comprehending the relationships between the structure and property of HOFs, providing valuable insights for the rational design of supramolecules tailored to specific applications [34, 37, 42, 43, 47–62].

In 2018, Schroder et al. described an example of "interpenetration isomerism" in three-dimensional HOFs [53]. By exploiting the crystallization conditions for a peripherally extended triptycene, (abbreviated as $H_6$PET, chemical formula: 4,4',4'',4''',4'''',4'''''-(9,10-dihydro-9,10-[1,2]benzenoanthracene-2,3,6,7,14,15-hexayl)hexabenzoic acid ($H_6$PET), they can modulate the interpenetration of the assembled frameworks, yielding a two-fold interpenetrated structure PETHOF-1 and a five-fold interpenetrated structure PETHOF-2 as interpenetration isomers (Fig. 5(a)). In PETHOF-1, two individual nets are related by inversion symmetry and form an interwoven topology with a large

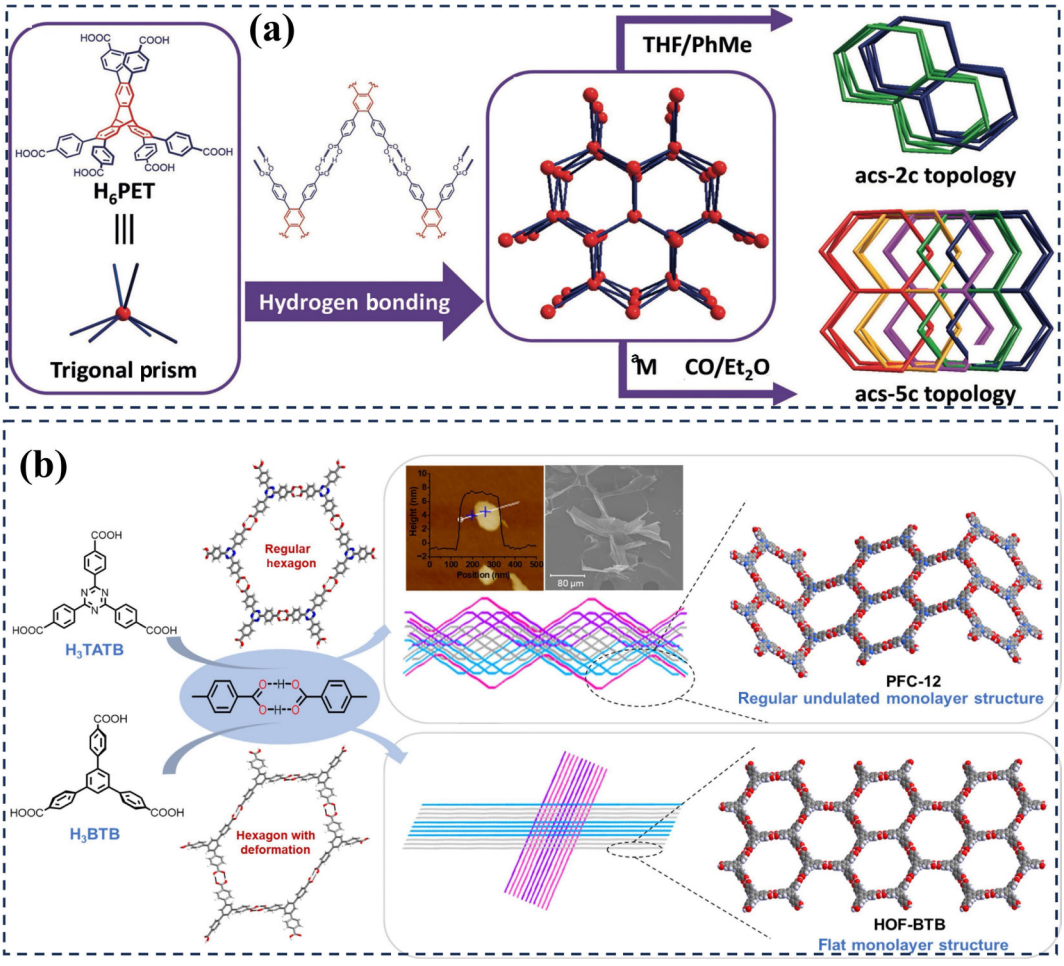


**Figure 5** (a) The assembly of a pair of "interpenetration isomers". Reproduced with permission from Ref. [53], © Wiley-VCH Verlag GmbH & Co. KGaA, Weinheim 2019. (b) Representation of the chemical structure, the obtained hexagonal honeycomb motifs, and the resulting monolayer and polycatenated networks constructed by $H_3$TATB (upper panel) and $H_3$BTB (lower panel). Reproduced with permission from Ref. [54], © American Chemical Society 2020.

guest-accessible volume of about 80%. In PETHOF-2, five individual nets are related by translational symmetry and are stacked in an alternating fashion. The activated materials (PETHOF-1a) showed permanent porosity with Brunauer–Emmett–Teller (BET) surface areas exceeding 1100 $m^2 \cdot g^{-1}$. It was found that the doubly interpenetrated PETHOF-1 was more stable than PETHOF-2 with a higher degree of interpenetration. Application of vacuum, even at 208 °C, resulted in complete loss of crystallinity in PETHOF-2, indicating superstructural instability, which can most likely be attributed to the highly strained hydrogen-bonded lattice. Synthetic control over the framework interpenetration could serve as a new strategy for constructing complex supramolecular architectures from simple organic building blocks.

By understanding the structure and properties of HOFs, we have utilized their multilevel structure to construct HOFs with intercalation. The structure of HOFs is dominated by molecular building blocks, which consist mainly of two indispensable parts: the backbone and hydrogen-bonding interactions. Changing either one of them could lead to a significant difference in the structure of the resulting materials [42, 59]. This motivated us to study ligands with identical hydrogen-bonding interactions but different backbone geometries. 4,4',4''-benzene1,3,5-triyltris (benzoic acid) ($H_3$BTB, also called 1,3,5-tris(4-carboxyphenyl) benzene and abbreviated as TCPB) and 4,4,'4''-(1,3,5-triazine-2,4,6-triyl)tribenzoic acid ($H_3$TATB), shown in Fig. 5(b), demonstrated such an example. $H_3$TATB is a planar molecule with a conjugate, and $H_3$BTB is a non-planar molecule. While PFC-12, a HOF constructed from $H_3$TATB, has structural undulations, HOF-BTB, constructed from $H_3$BTB, has no structural undulations (Fig. 5(b)) [63]. We hypothesized that the structural differences caused by these two similar ligands could be attributed to the slight twisting of the ligand $H_3$BTB, which led to a large structure change due to surface energy. The surface energy change gave PFC-11 and PFC-12 a distinctive stepwise adsorption behavior under a specific pressure that arose from the motion between the intertwined hexagonal networks. In addition, the structural variation led to interpenetration only in the HOF with $H_3$TATB, resulting in a difference in their stability—PFC-11 exhibited better stability than PFC-12 and PFC-13 [54].

**Chemically cross-linked HOFs.** Apart from the conventional strategies employed for constructing stable HOFs, researchers are actively exploring novel approaches, many of which have shown promising advancements. Ke et al. [64] devised hydrogen-bonded cross-linked organic frameworks ($H_C$OFs) by leveraging the advantages of COFs and HOFs (Fig. 6(a)). These frameworks offer significant chemical stability, enabling selective adsorption of environmentally impactful guests while introducing novel elastic properties to the prevailing crystalline porous organic materials. This approach initially involved the crystallization of molecular precursors through multivalent hydrogen bonding interactions, yielding potentially porous molecular materials akin to HOFs. Notably, the solvent molecules within the crystals can remain intact prior to the subsequent chemical cross-linking step, ensuring the covalent cross-linking of these well-organized molecules without compromising their crystallinity. This approach proved to enhance the chemical stability of the network.

**Charge-assisted H-bonds.** Incorporating charge-assisted

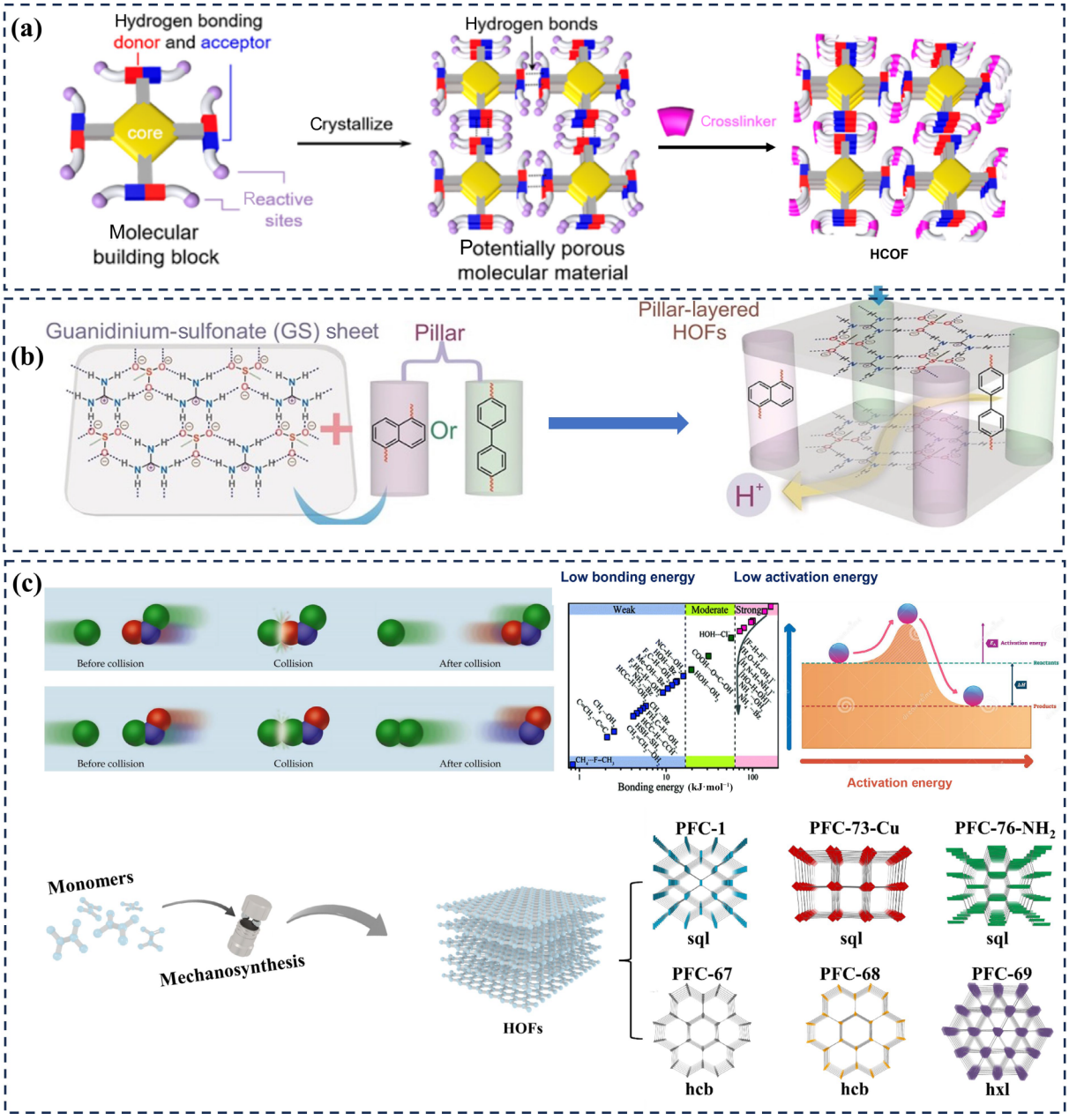


**Figure 6** (a) Illustration of the design of $H_C$OFs through SCSC transformation. $H_C$OFs possess guest-induced expandable voids because of the flexible cross-linkers. Reproduced with permission from Ref. [64], © American Chemical Society 2017. (b) Illustration of the design of charge-assisted H-bonds. Reproduced with permission from Ref. [65], © Wiley-VCH Verlag GmbH & Co. KGaA, Weinheim 2016. (c) Illustration of the design of mechanically synthesized HOFs. Reproduced with permission from Ref. [66], © Wiley-VCH GmbH 2022.

hydrogen-bonding interactions is another strategy employed to enhance the stability of HOFs. The charge interaction between ions can facilitate the construction of stable HOFs utilizing two ionic building blocks with opposing charges. In 2016, Ghosh et al. [65] reported two porous HOFs constructed using alkyne sulfonates and guanidinium ions (Fig. 6(b)). Thermogravimetric analysis (TGA) of HOF-GS-10 and HOF-GS-11 revealed an initial weight loss caused by the liberation of the adsorbed solvent guest molecules. These HOFs demonstrated exceptionally high proton conductivity ($0.75 \times 10^{-2}$ and $1.8 \times 10^{-2}$ S·cm$^{-1}$, respectively) under humidified conditions, attributed to their ionic skeleton and additional proton source (from the ionic backbones built through arene sulfonates and guanidinium ions) [67]. In addition, these compounds exhibited low activation energy and higher proton conductivity than other porous crystalline materials, such as MOFs and COFs, even under ambient conditions of low humidity and moderate temperature (30–320 °C). Furthermore, when HOF-GS-10 and HOF-GS-11 developed cracks on their crystal surfaces caused by elevated temperatures or other factors, their crystallinity can be restored by immersing the HOFs in their mother liquor (acetone/MeOH, p-xylene/MeOH). This work suggests that combining ionic building units in frameworks is a viable method for creating stable HOFs.

**Mechanical synthesis.** The conventional synthesis methods for HOFs, such as hydrothermal synthesis and environmental diffusion, often suffer from time-consuming procedures, limited reproducibility, and the introduction of impurities that disrupt the self-assembly process. These challenges are primarily attributed to the low bond energy and activation energy of H-bonds, making these bonds susceptible to structural heterogeneity (varied linkages, mismatched stacking) and H-bond formation with solvents. Recently, our research group developed a novel synthesis method to overcome these problems. According to collision theory, successful collision reactions between molecules require adequate energy in the correct direction. Due to their limited energy, molecules often cannot induce effective collisions to form

covalent and coordination bonds, as these bonds possess relatively high activation energies. On the other hand, H-bonds are more likely to form through mechanical collisions due to their low activation energy. The presence of π–π interactions can also guide the direction of molecular collisions to form H-bonds. Building upon this concept, we have successfully synthesized a series of HOF structures using a ball-milling method (Fig. 6(c)), following a topologically predicted assembly approach [66]. This method allows for lattice-based HOF preparation with minimal reliance on solvent-assisted synthesis. The stability of the frameworks was effectively enhanced by eliminating solvents in the self-assembly process.

Moreover, the existence of a large number of hydrogen donor/acceptor groups (such as hydroxyl, amine, and pyrazole) in HOFs allowed them to bind with various exogenous species to fabricate HOF-based derivatives. For example, by adding Pd precursors in the reaction mixture, a series of HOF-based composites, denoted as Pd@HOFs, were synthesized through a one-pot mechanosynthesis method [66]. The highly ordered HOF matrix not only acted as a surfactant to prevent nanoparticles from aggregating, but it also served as a porous substrate integrating various functional groups that enhanced mass transfer. The one-pot ball-milling synthesis method we developed is featured by its simplicity, cost-effectiveness, efficiency, and ease of obtaining nano morphs. This method also exhibited a certain degree of universality for different HOFs and scalability for production.

As shown above, various strategies have been utilized to synthesize stable HOFs with unique properties for different applications. As stable HOFs obtained using different methods may exhibit different structure features and properties, it is crucial to select the appropriate synthetic method for HOFs of interest. For instance, the adoption of π–π stacking may facilitate the construction of stable HOFs with catalytic capabilities, as π–π stacking can effectively induce charge transfer. Stable HOFs with charge-assisted H-bonds are suitable for gas storage and separation, leveraging their ionic channels [68]. Highly interpenetrated and chemically cross-linked stable HOFs can take advantage of the pore segmentation resulting from these strategies and also find application in gas storage and separation. Mechanical synthesis proves to be instrumental in fabricating nanosized HOFs tailored for biomedical applications. The careful selection of these strategies can lead to stale HOFs with desirable structures and properties for target applications.

In addition to these reported methods, researchers are actively exploring new synthetic strategies to craft stable HOFs with tailored properties for diverse applications.

## 3 Photo-response of HOFs

### 3.1 Photocatalysis

The production of renewable fuels from solar energy and abundant resources, such as water and carbon dioxide, through photocatalytic reactions is considered a promising strategy to address the climate challenge adequately [69, 70]. Photocatalytic systems based on porous materials have been studied to convert solar energy into hydrogen and other solar fuels. MOFs are common porous materials used for photocatalysis. However, the relatively low conductivity of MOFs requires the selection of suitable sacrificial agents. The modification of band positions by selecting appropriate linkers may be a way to improve the photocatalytic performance of porous materials, as exemplified by the recent development of COFs photocatalysts [71–77]. COFs can be viewed as pure linker frameworks, and one can tune band edges and porosity of COFs for a chosen application by selecting the appropriate linkers. Nevertheless, the harsh synthesis conditions of COFs limit their large-scale industrial production.

To this end, our group has analyzed how the preparation method could affect the structural properties and catalytic activity of HOFs. Based on the structure–activity relationship established, we have been optimizing the preparation method of porous HOFs by adjusting catalyst loading and morphology. In 2021, we combined metal catalytic sites with photosensitizers and investigated different metals to increase the stability of the framework and improve the $CO_2$ reduction activity (Fig. 7(a)) [78]. When using the designed HOFs as the catalysts, we determined that CO is the only product of the reaction through

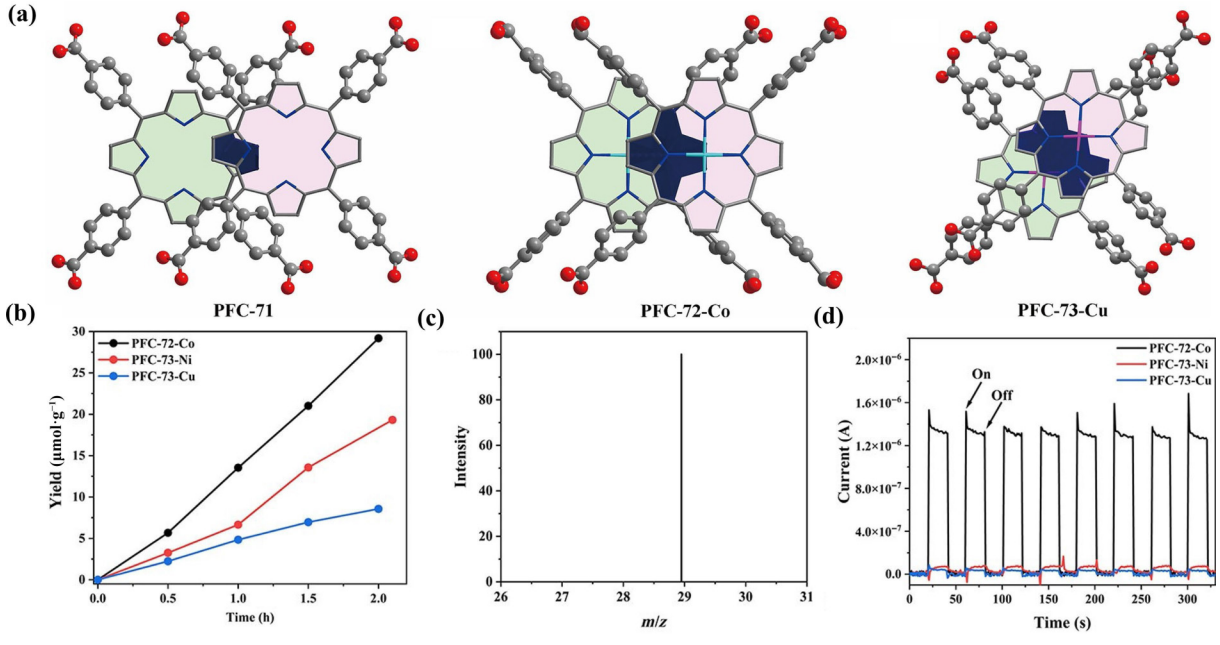


**Figure 7** (a) Schematic of interlayer porphyrin center-to-center distance and orbital overlap area highlighted in dark blue (hydrogen atoms are omitted for clarity). (b) Time-resolved CO productions of photocatalytic $CO_2$ reduction over PFC-72-Co, PFC-73-Ni and PFC-73-Cu; (c) mass spectrum of produced $^{13}CO$ via isotope $^{13}CO_2$ reduction under visible light; (d) transient photocurrent response of PFC-72-Co, PFC-73-Ni, and PFC-73-Cu. Reproduced with permission from Ref. [78], © Wiley-VCH GmbH 2021.

gas chromatography and ion chromatography. Among them, PFC-72-Co showed the best performance (14.7 μmol·g$^{-1}$·h$^{-1}$), 1.5 times higher than PFC-73-Ni (9.8 μmol·g$^{-1}$·h$^{-1}$) and 3 times higher than PFC-73-Cu (4.4 μmol·g$^{-1}$·h$^{-1}$) times (Fig. 7(b)).

In addition, the performance of a photocatalyst depends on the photosensitizer's light-trapping ability and the charge transfer efficiency between the photosensitizer and the catalyst. Powder catalysts have poor visible light utilization due to aggregation and, thus, low photocatalytic efficiency. To tackle this problem, we synthesized a non-homogeneous structure by integrating $Cu_2O$ with a new porphyrin HOF, PFC-45 [79]. The heterogeneous p-type $Cu_2O$ and n-type HOF network showed higher charge separation efficiency. An efficient thin-film photocatalyst (PFC45/$Cu_2O$@CP) with this inhomogeneous structure was developed using electrophoresis deposition (EPD) technology (Figs. 8(a) and 8(b)). The results show that the PFC-45/$Cu_2O$ hetero-structured film has high selectivity and activity in catalyzing the photoreduction reaction of $CO_2$ to CO in pure water with a CO yield of 11.81 μmol·g$^{-1}$·h$^{-1}$.

Furthermore, inspired by the natural polystyrene bioprocess, we considered integrating a sufficient number of photosensitizers and an appropriate number of catalytic centers in one multiphase catalyst. This biomimetic multiphase catalyst was synthesized by self-assembling metalloporphyrin monomers into HOFs, in which the ratio of photosensitizer to catalytic centers can be adjusted by changing the percentage of metalloporphyrin centers in this prototype structure (Fig. 8(c)). The combination of experimental and computational results showed that changing the metalloporphyrin content not only achieved the fine-tuning of the photosensitizer/catalyst ratio but also significantly changed the microenvironment (e.g., electron density, substrate-skeleton interaction, and redox potential) and charge separation efficiency around the active center (Fig. 8(d)) [80].

**Photocatalytic hydrogen production.** Photocatalytic hydrogen production is considered a viable strategy for effectively using solar energy to solve the growing environmental and energy problems. With ordered structures, tunable pore sizes, and large specific surface areas, HOFs integrated with photoactive moieties are excellent photocatalysts for this application. The well-defined structures of HOFs can also facilitate studying structure–property relationships for these materials, which may provide insights into the photocatalytic mechanisms of HOF-catalyzed hydrogen production.

For this purpose, we integrated a photoactive graphitic carbon nitride ($C_3N_4$) part in a HOF structure (PFC-42) with high porosity and crystallinity (Fig. 9(a)) [81]. Under visible light irradiation, PFC-42 loaded with Pt nanoparticles (PFC-42-Pt) produced hydrogen continuously from water in the presence of TEOA scavenger at a rate of 11.32 mmol·g$^{-1}$, which is the highest among the reported Pt/porous composites. The superior $H_2$ precipitation rate of PFC-42-Pt compared to the amorphous analog $C_3N_4$-Pt and the nanosheet $C_3N_4$-Pt indicates that the ordered arrangement of the photosensitizer can significantly improve the photocatalytic activity of the material.

Conjugated organic photocatalysts generally exhibit broader light absorption but often suffer from relatively low apparent quantum yield (AQY). The low AQY may be attributed to the strong Coulomb attraction between positive and negative charges generated by organic semiconductors under irradiation, characterized by high exciton binding energies (typically > 0.1 eV). The high exciton binding energy means excitons must diffuse to the semiconductor surface to dissociate into carriers. However, most organic semiconductors have short exciton diffusion lengths (typically 5–10 nm), resulting in higher recombination rates and poor exciton dissociation [82, 83].

In 2023, Zhu et al. employed transient spectroscopic methods to investigate the effect of micropores on exciton behavior [84]. Their method combines visible-mid-infrared femtosecond transient absorption spectroscopy (TAS) and time-correlated single-photon counting (TCSPC), which enabled them to study how the exciton transfer path of HOF-$H_4$TBAPy was affected by its 1D micropore channels. In addition, the impact of the internal active adsorption region was further investigated using crystal engineering, specifically by controlling the length of the 1D channel. They also performed first-principles calculations and attenuated total reflection Fourier transform infrared (ATR-FTIR) spectroscopy to study the reaction sites in the channels of the HOF. By controlling the one-dimensional channel length (≤ 0.59 μm), they found that micropore-confined excitons played a dominant role in photocatalysis and obtained a significantly enhanced $H_2$ evolution rate of 358 mmol·h$^{-1}$·g$^{-1}$ (537 μmol·h$^{-1}$; Fig. 9(g)).

### 3.2 Photodynamic and photothermal therapy

Photothermal therapy (PTT) is an effective cancer treatment method that utilizes light-absorbing materials to convert near-infrared (NIR) light energy into heat. This localized heat generation selectively eradicates cancer cells while minimizing damage to healthy tissue. PTT has gained significant attention in biomedical applications due to its minimally invasive nature. Although chemotherapy is a widely used and relatively reliable cancer treatment, mitigating its side effects is crucial. The combination of chemotherapy and PTT holds promising potential due to their synergistic effect, which enables a reduced dosage of chemotherapeutic agents to be effective and mitigates their associated adverse effects [85–91]. Hence, developing multifunctional biocompatible and biodegradable nanoplatforms integrating chemotherapy and thermotherapy holds significant potential for clinical cancer treatment. Photodynamic therapy (PDT) is an oncological treatment that has great potential due to its spatio-temporal specificity and non-invasive nature. PDT kills tumor cells directly by using reactive oxygen species and also induces an anti-tumor immune response through immune action.

With this objective in mind, in 2020, we pursued the integration of porphyrin photosensitizers as porous backbones and commercial bactericides as counterion (QA ions) into the structure [92]. PFC-33 demonstrated ion-responsive release behavior in diverse physiological environments, resulting in synergistic photodynamic and chemical antimicrobial efficacy. During membrane fabrication, the unbound carboxyl groups on the HOF surface enable precise control over the interfacial interactions between PFC-33 and the polymer matrix. Consequently, the poly-HOF membranes achieved excellent stability, desirable flexibility, and high permeability, exhibiting high efficacy in inhibiting E. coli growth (Fig. 10(a)). Moreover, the photo-responsive nature of HOFs allows for preparing wearable items. Li et al. reported the preparation of broad-spectrum antimicrobial nanofibers using electrospinning, which incorporated a photoactive HOF consisting of rod-shaped nanocrystals measuring approximately 60 nm in length [93]. The resulting HOF@PVDF-HF nanofibers exhibited excellent tensile strength and breathability, protecting the HOF nanocrystals from acid and alkali corrosion (Fig. 10(b)). A series of nanofibers were prepared to optimize the efficiency of singlet oxygen ($^1O_2$) generation, incorporating varying amounts and types of HOF nanocrystals. It was found that the nanofibers containing 0.5 wt.% HOF-101-F@PVDF-HFP demonstrated the highest efficiency in $^1O_2$ generation, exhibiting an enhancement of nearly two times compared to the HOF-101-F microcrystalline powder. The HOF@PVDF-HFP nanofibers effectively eliminated various pathogens, including viruses, bacteria, and fungi, within 30 min

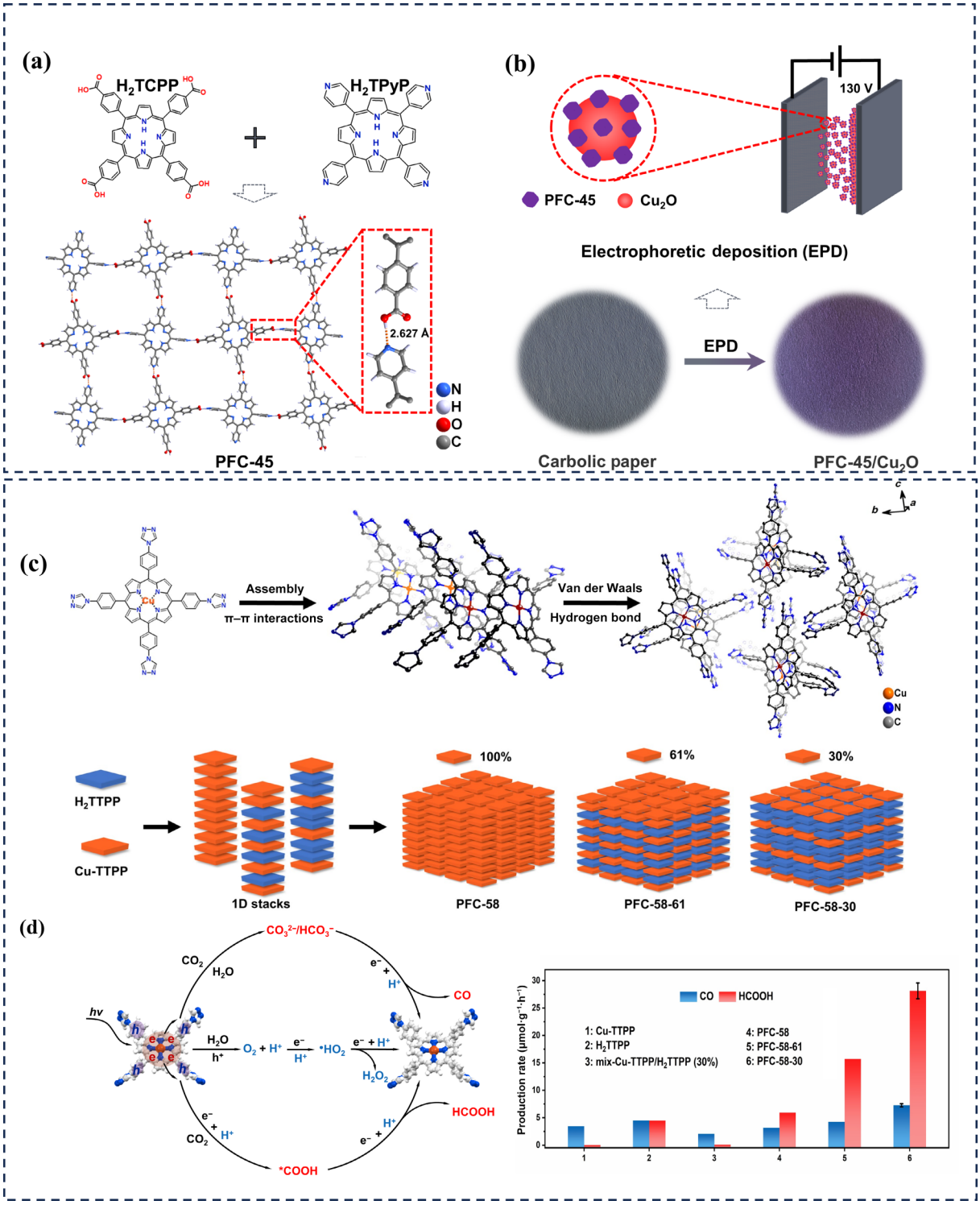


**Figure 8** (a) Structure and the connection of adjacent building blocks in PFC-45. (b) Schematic illustration of the designed synthetic process for the PFC-45/$Cu_2O$ film on CP using EPD. (c) Crystal structure of PFC-58 composed of porphyrin building blocks with AA packing mode. Schematic diagram of the structures of PFC-58 series HOFs with different metalloporphyrin contents. Reproduced with permission from Ref. [79], © American Chemical Society 2022. (d) Proposed mechanism for the $CO_2$ photoreduction of PFC-58-30 and the C-NMR spectra for HCOOH obtained by using $^{13}CO_2$ or $^{12}CO_2$ as a reactant in the reaction catalyzed by PFC-58-30. General procedure: 5 mg photocatalyst and 3 mL water were irradiated by visible light > 400 nm using an Xe lamp with filters. Reproduced with permission from Ref. [80], © Wiley-VCH GmbH 2022.

under ambient light conditions.

Near-infrared light therapy is widely recognized as highly effective; however, finding materials that emit near-infrared light, particularly framework materials, is challenging. With the goal of developing such materials, in 2021, we synthesized the first core–shell heterostructure up-conversion nanoparticles (UCNPs) and HOFs using a "bottle-around-ship" strategy combined with a stepwise ligand grafting approach [94]. The crystalline porous network can maintain a persistent radical state when exposed to visible light irradiation [95–97], demonstrating photothermal and photodynamic capabilities (Fig. 11(a)). Specifically, we selected B-NaYF4: Yb, Er UCNPs with an emission trap overlapping with the PFC-55 excitation wavelength. These UCNP materials were used to create a core–shell structure with PFC-55, enabling the utilization of near-infrared light energy for resonant energy transfer (RET) processes. This approach prevents the independent

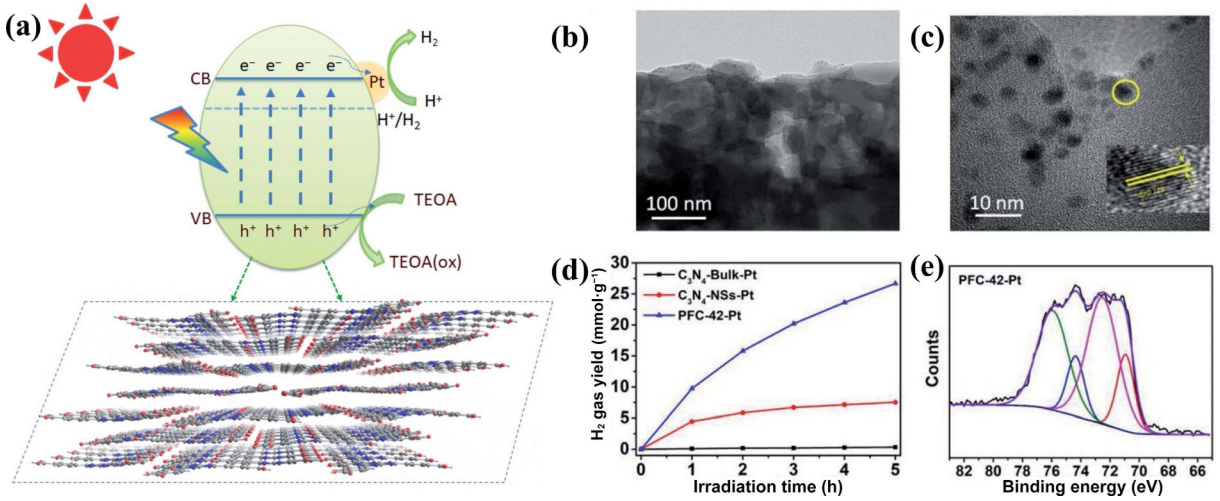


**Figure 9** (a) The proposed mechanism for visible-light-driven photocatalytic $H_2$ production with PFC-42. (b) TEM micrographs of PFC-42 with the uniform distribution of Pt nanoparticles. (c) High-resolution TEM image of 3–5 nm Pt nanoparticles on PFC-42, showing the planes of Pt with the d spacing of 0.229 nm. (d) Photocatalytic $H_2$ generation activity of bulk $C_3N_4$-Pt, sheet $C_3N_4$-Pt, and PFC-42-Pt under the same reaction conditions. (e) High-resolution Pt 4f XPS spectrum. Structure of HOF-$H_4$TBAPy. Reproduced with permission from Ref. [81], © Royal Society of Chemistry 2021.

nucleation of physical mixtures and yields a uniform core–shell structure known as UCNPs@PFC-55. The core–shell heterogeneous structure facilitated the up-conversion of near-infrared light (980 nm) into the visible region (540 and 653 nm) by the UCNPs "core", capable of deep tissue penetration (Fig. 11(b)) [98, 99]. Subsequently, the PFC-55 "shell" is excited, leading to a notable photothermal effect and the generation of $^1O_2$ through the RET process (Figs. 11(b) and 11(c)). Therefore, the core–shell nanostructures based on HOFs exhibit substantial antimicrobial efficiency, resulting from the combined near-infrared responsive photothermal and photodynamic effects. These structures demonstrate promising potential for wound disinfection and biofilm ablation [100].

Compared with coordinate and covalent bonds, hydrogen-bonding interactions are intrinsically more flexible, weaker, highly reversible, and of low directionality, which endow HOFs with many unique advantages such as good solution processability, mild synthesis conditions, and multiple responsiveness. Besides, since HOFs are metal-free, the underlying harmful effect of metal ions on biological settings could be circumvented. These unique characteristics provide HOFs with great potential as a tunable platform for constructing multi-functional materials that are urgently needed for biomedical applications. For example, Falcaro et al. [101] have reported a biocompatible HOF, BioHOF-1, that can readily encapsulate two native enzymes and keep them active beyond biological conditions. More importantly, the strength of H-bonding spanned a large range in these HOFs. Relatively weak hydrogen bonding is more vulnerable to thermal stimulus. Thus, manipulation of the overall crosslinking force in HOFs can be realized by properly introducing multiple types of hydrogen bonds with different bonding strengths (i.e., hierarchical hydrogen bonds). Given these properties, HOFs have the potential to serve as a novel artificial exoskeleton for living cells, providing them with robust protection against severe chemical and physical lethal stressors, and showing the possibility of spatiotemporally controllable degradation upon NIR-II laser irradiation.

In 2022, Qu et al. [102] presented a new way to encapsulate neural stem cells (NSCs) by using HOFs to overcome the common causes of low therapeutic efficacy during NSC transplantation, including (1) loss of fundamental stem cell properties, "stemness", before transplantation, (2) cytomembrane damage during transplantation, and (3) apoptosis due to oxidative stress after transplantation. Porous carbon nanospheres (PCNs) were doped into the HOF shell during the process of mineralization to endow the cellular exoskeletons with hierarchical hydrogen bonds and the ability to resist oxidative stress due to the catalase and superoxide dismutase-like activities of PCN. Under NIR-II irradiation, thermal-responsive hydrogen bonds dissociated to release NSCs. Stereotactic transplanting encapsulated NSC into the brain of an Alzheimer's disease (AD) mouse model further verified that their design can enhance NSC viability, promote neurogenesis, and ameliorate cognitive impairment.

### 3.3 Mimicking photo-responsive enzymes using HOFs

The activity of some enzymes relies on light-harvesting cofactors located in the active site. These cofactors facilitate the transfer of electrons or protons during irradiation, leading to complex biotransformation processes. The molecules that form the structure are interconnected, which can alter the internal electric field and energy gap. Furthermore, an extended π–π conjugated system likely enhances electron transfer. It suggests that conjugated crystal systems with a crystalline structure have greater photosensitivity than monomers, which is supported by the observed increase in photocurrent density during switching cycles. Flexible porous framework materials with adjustable structures, like HOFs, hold promise for advancing photo-responsive enzymes [103, 104].

Considering this, Chen et al. [105] reported the pore environment-dependent, photo-responsive oxidase activity in three isostructural HOF nanozyme (Bovine albumin, BSA). They first sought out a series of photo-active carboxylate tectons suitable for the linkage into a HOF with an explicit structure and identified the tecons to have the best light-harvesting ability using density functional theory (DFT) calculation (Figs. 12(a) and 12(b)). According to the theoretical predictions, three photo-responsive isostructural HOF nanozymes possessed similar band gaps and generated comparable reactive oxygen species (ROS) under visible light irradiation. Remarkably, the photo-responsive oxidase activity, commonly considered ROS-dependent, drastically differed in these three HOFs. This variation in oxidase activity was demonstrated to be associated with the substrate-pore interaction, reminiscent of the binding effect of the native enzyme pocket that mediates the biocatalysis.

### 3.4 Photochromic materials incorporating HOFs

Photochromic materials are intelligent substances that alter their

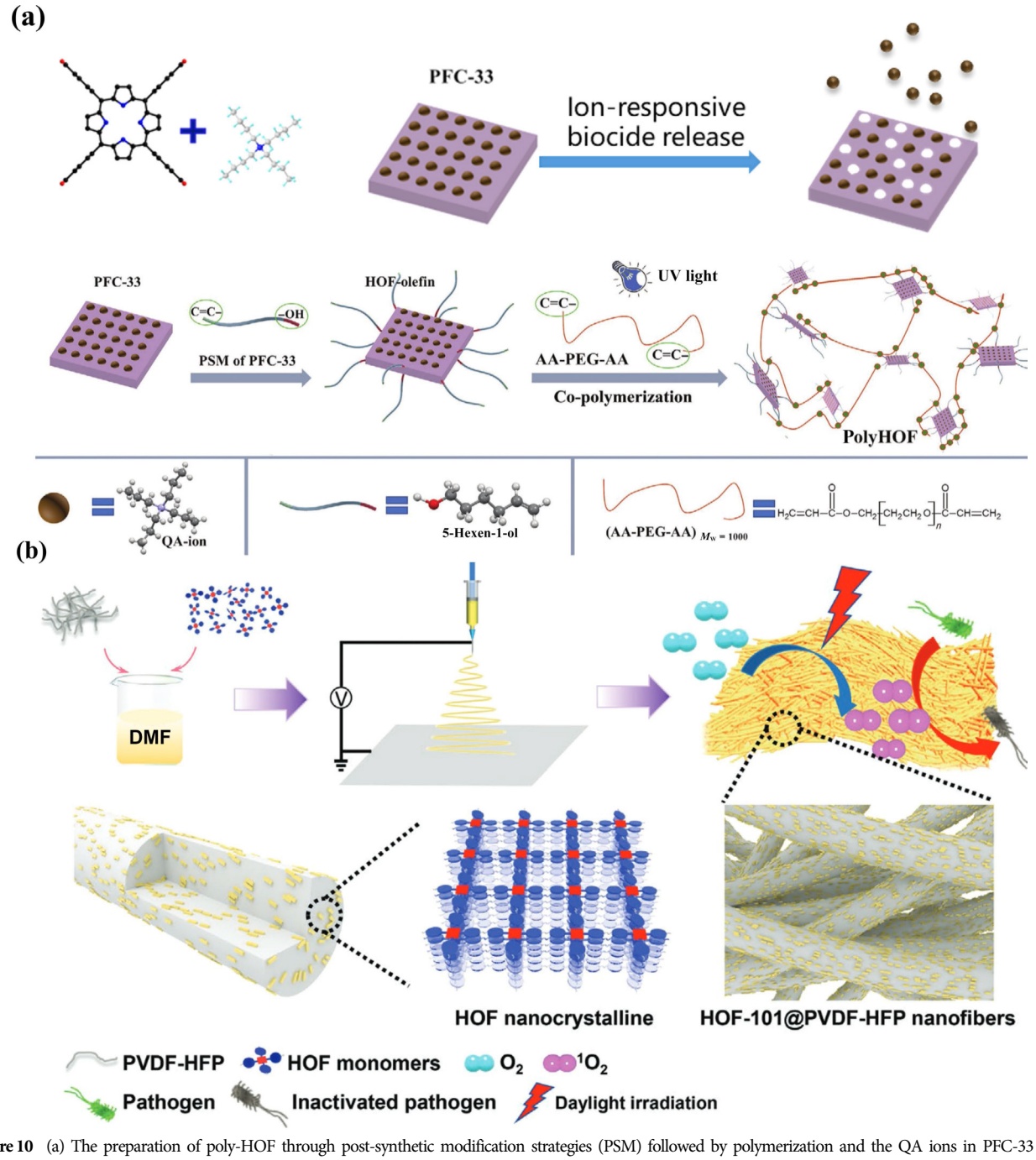


**Figure 10** (a) The preparation of poly-HOF through post-synthetic modification strategies (PSM) followed by polymerization and the QA ions in PFC-33 were released over time in water. Reproduced with permission from Ref. [92], © Wiley-VCH GmbH 2020. (b) A schematic showing the preparation of antibacterial HOF@PVDF-HFP nanofibers and the antibacterial mechanism. Reproduced with permission from Ref. [93], © Wiley-VCH GmbH 2023.

appearance or emit colors in response to external stimuli. These materials hold great potential for applications in anti-counterfeiting measures. However, the majority of these materials demonstrate two-color transitions, low-contrast emission, or prolonged transition periods, rendering them impractical for real-world applications. HOFs with flexible framework structures exhibit superior responsiveness to external stimuli compared to COFs and MOFs. This characteristic positions HOFs as promising candidates in the field of photochromic materials.

Yang et al. [106] introduced a novel method involving the combination of a widely-used photochromic molecule, spiro pyran (SP), with HOFs (Fig. 13(a)). This approach enabled the reversible switching of SP in solid states and demonstrated dynamic displays of encrypted information. The composite system offers several advantages: (1) it exhibited diverse dynamic fluorescence emission and visible colors that are regulated by high-contrast ultraviolet radiation and can be reversibly converted; (2) these behavioral changes can be easily achieved through simple UV illumination; and (3) in contrast to prior studies, this work not only demonstrated dynamic fluorescence emission but also revealed dynamic information during the decryption process (Fig. 13(b)).

Ultralong organic phosphorescent (UOP) materials without any metal species exhibit significant potential for applications in optical technologies and biological imaging, owing to their low cost and biocompatibility. Nevertheless, preparing new UOP materials with extended luminous lifetimes and high photoluminescence quantum yields (PLQYs) remains a challenge [107]. Our group employed supramolecular self-assembly to combine two organic molecules, namely, the high PLQY compound 1,4-phenylene diboric acid (PBA) and the long-lived isophthalic acid (IPA), resulting in the formation of two crystalline

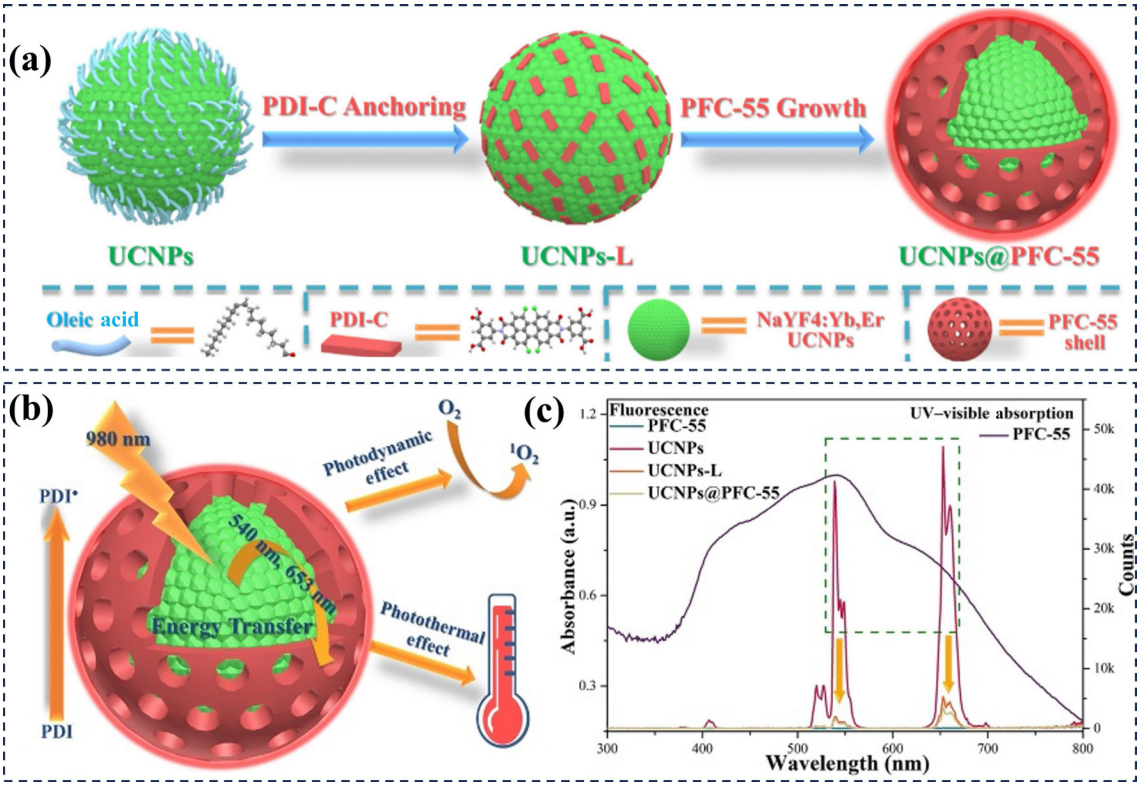


**Figure 11** (a) Fabrication of core–shell UCNPs@PFC-55. (b) The RET process from UCNPs "core" to PFC-55 "shell" for achieving NIR-response photo-thermal and photodynamic effects. (c) UV–visible absorption spectrum of PFC-55 (energy acceptor); and the up-conversion photoluminescence spectra of UCNPs (energy donner), UCNPs-L, and UCNP@PFC-55 exited by 980 nm. Reproduced with permission from Ref. [94], © Wiley-VCH GmbH 2021.

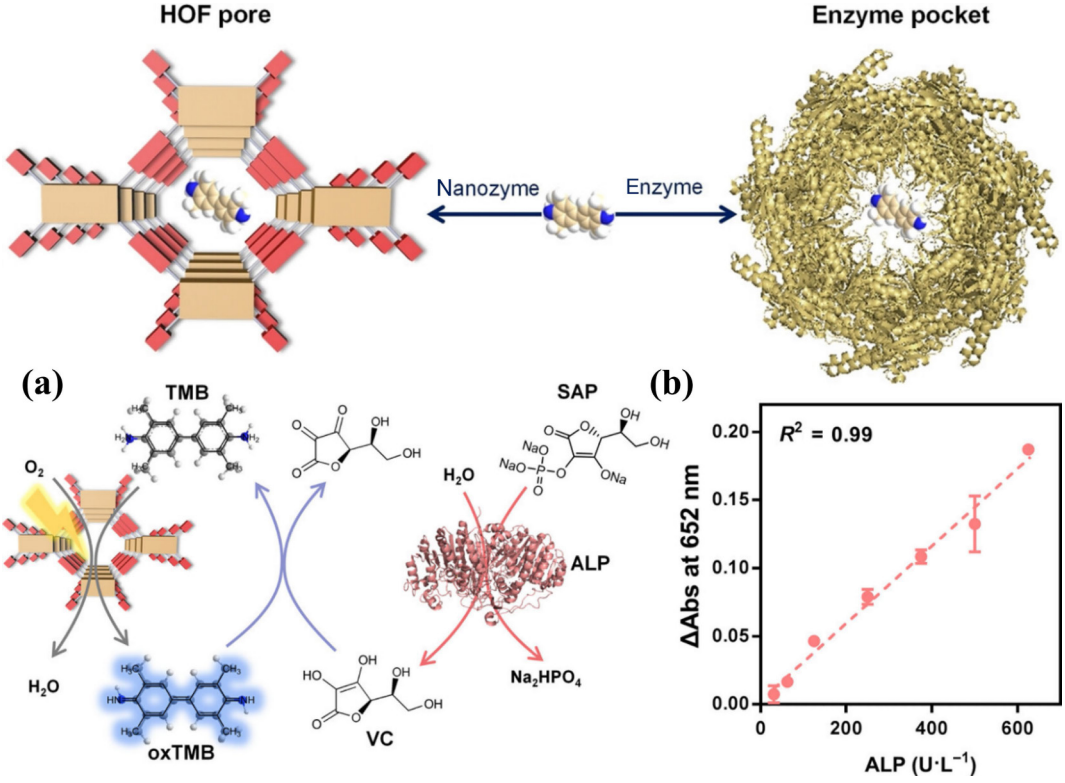


**Figure 12** Schematic representation of the substrate-pore interaction in HOF pore and enzyme pocket. (a) Schematic representation of the ALP sensing mechanism using this photo-responsive HOF-101 nanozyme. (b) The linear range for ALP quantification. Reproduced with permission from Ref. [105], © Wiley-VCH GmbH 2023.

hydrogen-bonded organic chains named PBA-IPA1 and PBA-IPA2 (Fig. 13(c)). PBA-IPA2 exhibited significantly enhanced phosphorescent lifetime (1.59 s) and PLQY (15.72%) compared to PBA-IPA1, attributed to the triplet–triplet energy transfer between the two components, further supported by computational studies. The resulting material holds potential for applications in areas such as information encryption and fingerprint identification, offering a novel approach to designing UOP materials with practical uses (Fig. 13(d)).

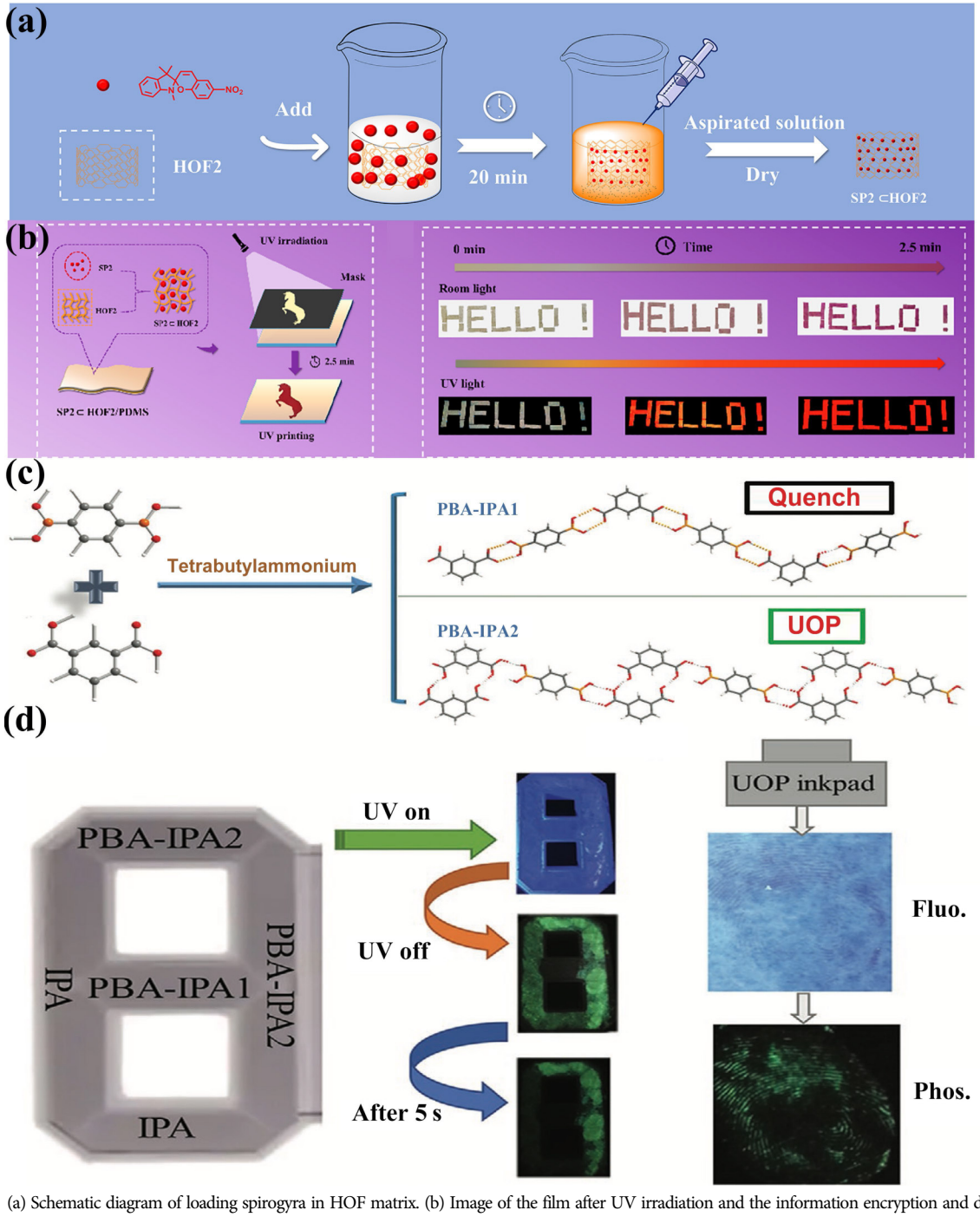


**Figure 13** (a) Schematic diagram of loading spirogyra in HOF matrix. (b) Image of the film after UV irradiation and the information encryption and decryption in view of $SP^2$ ⊂ HOF2/PDMS film. Reproduced with permission from Ref. [106], © American Chemical Society 2022. (c) Design of two hydrogen-bonded organic chains PBA-IPA1 and PBA-IPA2. (d) Optical images of the UOP materials. A plastic digital 8 model filled with different UOP materials showing digits 8, 0, 7 sequentially with 365 nm UV light on and off. The luminescent fingerprint images with UOP inkpad under UV excitation and after stopping UV excitation. Reproduced with permission from Ref. [107], © Wiley-VCH Verlag GmbH & Co. KGaA, Weinheim 2020.

### 3.5 Photo-responsive electron and proton conductivity

Achieving simultaneous multiple functions in a single material has been a significant challenge, as individual functions are often difficult to correlate. Consequently, developing a single organic co-crystal/HOF material with multiple functions has been scarcely explored, despite the crucial importance of these multifunctional properties for practical applications. For instance, a material capable of simultaneously conducting electrons and protons could find applications in various fields, including organic electrochemical transistors, batteries, light-emitting electrochemical cells, chemical sensors, neuromorphic modules, bioelectronic probes, and ion pumps [108].

Recently, Zhang et al. [109] reported a 2D HOF denoted as HOF-FJU-36, based on a donor–acceptor (D–A) π–π stacking architecture (Fig. 14(a)). The framework involved the zwitterionic acceptor 1,1'-bis(3carboxybenzyl)-4,4'-bipyridinium ($H_2L_2^+$) and the donor 2,7-naphthalene disulfonate (NDS-2). Three water molecules were positioned within the channels, establishing hydrogen bonding interactions with acidic species, and contributing to forming a 3D framework. π–π interactions along *a* axis and a continuous hydrogen bonding chain along the *b* axis served as electron and proton transfer pathways, respectively (Fig. 14(c)). Upon irradiation with 405 nm light, the photogenerated radicals confer photo-switchable electron and proton conductivity to HOF-FJU-36 through coupled electron–proton transfer (Fig. 14(b)). The mechanism behind the irradiation-induced switchable

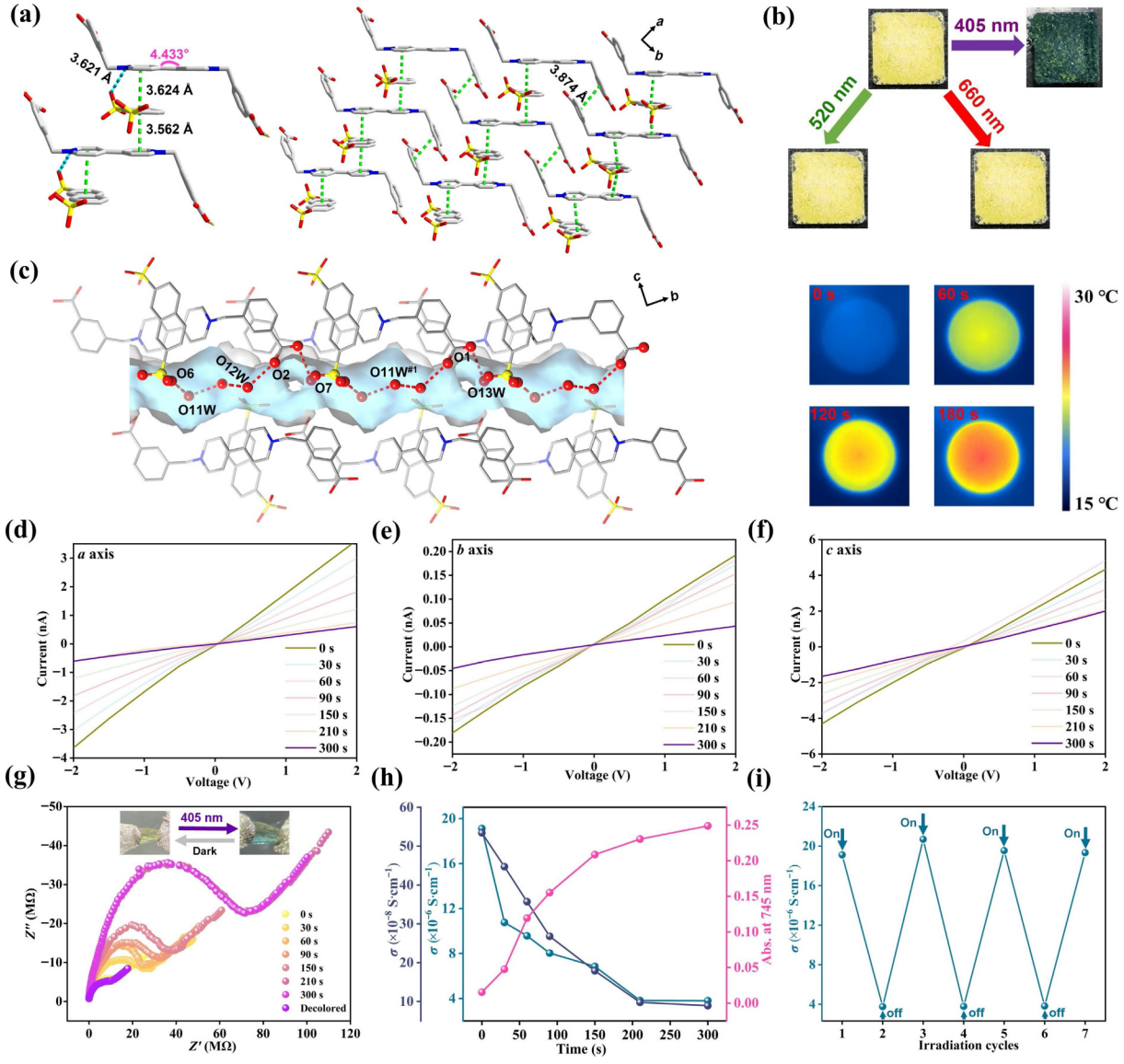


**Figure 14** Crystal structure of HOF-FJU-36. (a) Asymmetric unit of HOF FJU-36. (b) 2D layers formed by infinite π–π interactions of HOF-FJU36. (c) Schematic representation of proton conductive path in the hydrogen-bonded chain. Parts of H atoms are omitted for clarity. Three-dimensional stack for hydrogen bonding chain fragment along the *b* axis. Symmetry codes: 2 + *x*, 2 + *y*, 1 + *z*. Color changes in HOF-FJU-36 upon 405, 520, and 660 nm laser irradiation. Time-dependent current–voltage (*I*–*V*) curves of HOF-FJU-36 single crystal along (d) *a* axis, (e) *b* axis, and (f) *c* axis upon 405 nm laser irradiation in air. (g) Time-dependent Nyquist variation plots along the *b* axis upon 405 nm laser irradiation in air. Insert the Reversible switch of a single crystal between before and after illumination. (h) Plots of irradiation time vs. electron conductivity for HOF-FJU-36 single crystals along *a* axis, proton conductivity along the *b* axis, and absorbance at 745 nm. (i) Photo switching proton conductivity of HOF-FJU-36 for repeated cycles in air. Reproduced with permission from Ref. [109], © Wiley-VCH Verlag GmbH 2023.

conductivity has been elucidated through single-crystal X-ray diffraction (SC-XRD) analyses, X-ray photoelectron spectroscopy (XPS), transient absorption spectra, and density functional theory calculations (Figs. 14(d)–14(i)).

### 3.6 Photo-response synergizes with external stimulus-response

The unique dynamics and versatile applications of flexible hydrogen-bonded organic frameworks (FHOFs) have garnered significant attention. However, to mitigate potential issues with framework stability resulted from the relatively fragile nature of hydrogen bonds, most previous studies have focused on employing various strategies to construct robust and rigid HOFs [110]. These robust/rigid HOFs can maintain their original porous structures without undergoing any changes when exposed to external stimuli. In contrast, FHOFs are characterized as having the ability to undergo reversible structural transformations in response to external stimuli while preserving their crystalline nature [35, 50, 111–113]. Despite the greater challenges in synthesizing stable FHOFs, their dynamic behaviors gradually garner more attention from the scientific community. Generally, at the very least, FHOFs should only lose the long-range order of their frameworks without transitioning into amorphous states throughout the entire stimuli-responsive process [114, 115]. To induce reversible stimuli-responsive motions, FHOFs are typically constructed using flexible organic building blocks and weak hydrogen bonds. These design principles give rise to unique properties that are challenging to achieve in robust frameworks. It is worth noting that FHOFs generally exhibit a certain degree of stability, and their structures can undergo reversible transformations in specific environments while maintaining relative stability before and after the transformation. The reversible structural transformations of FHOFs, accompanied by changes in pore sizes and shapes in response to various factors such as guest molecules, temperature, and mechanical pressure, confer significant advantages in diverse applications. These applications include gas separation, luminescent sensors [116], host-guest chemistry [117], memory devices [118], and others.

**Synergistic photo- and thermal-responses.** Compared with coordinate and covalent bonds, hydrogen-bonding interactions are intrinsically more flexible, weaker, highly reversible, and of low directionality, which endow HOFs with many unique advantages such as good solution processability, mild synthesis conditions, and multiple responsiveness. The flexibility inherent in the HOF framework can result in the distortion of molecular chains within the building unit region when exposed to external thermal stimuli, thus altering the configuration of the HOF [68]. Consequently, this change in configuration can impact the electron transfer process within the HOF, subsequently influencing its luminescence performance. For example, Chi et al. developed the first example of a FHOF with local dynamics (named 8PZ) for adaptive guest accommodation through incorporating soft ethylester chains [110]. In the presence of various external stimuli such as solvents and temperature, local motions of ethyl-ester chains could occur, including in-plane and out-of-plane motions, which can efficiently regulate the pore size of 8PZ without significant changes in cell volumes and molecular assembling forms. Moreover, through the local dynamics, 8PZ can adapt to a series of 3-alkylthiophenes with large-scale alkyl-chain-length variation (Figs. 15(d) and 15(e)). Ten host–guest cocrystals suitable for SXRD analyses were further produced, which presented programmable temperature-dependent luminescence properties and showed great potential for microscale luminescent thermal alarms and multiple information encryption with logic programming (Fig. 15(b)). As a multifunctional smart platform, the FHOF, 8PZ, with local dynamics, is also promising for applications in sensing, separation, catalysis, biomedical imaging, optoelectronic devices, and many others. The employment of FHOFs with local dynamics as hosts in host–guest cocrystals should also provide a valuable strategy for the preparations of functional cocrystals. This work not only deepened our understanding of the relationship between framework structures and flexibilities of HOFs but also provided a hopeful avenue to engineer future multifunctional FHOFs with enriched applications.

Recently, Zhang et al. [119] reported the first smart-responsive HOF heterostructure with multiple spatial-resolved emission modes as a covert photonic security platform via differentiated design on high-electronegative atoms. HOF heterostructures were prepared by integrating different HOFs into a single microwire based on a hydrogen-bond-assisted epitaxial growth procedure. Adopted HOFs with different substitution positions of high-electronegative atoms exhibited distinct responsive characters, which endowed HOF heterostructures with both the thermochromism via the framework transformation and the acidichromism via the protonation effect, leading to multiple emission modes. Dual-stimuli-controlled emission modes and spatial-resolved emission behavior constituted a fingerprint of the heterostructure, which allowed for realizing smart-responsive photonic barcodes with multiple convert states, further demonstrating the dynamic coding capability and enhanced security as anticounterfeiting labels.

These results provide a promising route for the function-oriented design of smart-responsive HOF heterosystem, which may serve as a novel platform for optical data recording and information encryption.

**Synergistic photo- and pressure-responses.** Bionic sensors have played a significant role in the advancement of smart robots, medical equipment, and flexible wearable devices. The luminescent pressure-acoustic bimodal sensor can be regarded as an exceptional multifunctional integrated bionic device. Owing to its flexible and porous properties, HOF shows promising prospects for development in wearable devices and bionic devices.

Recently, Yan et al. [120] successfully synthesized flexible and

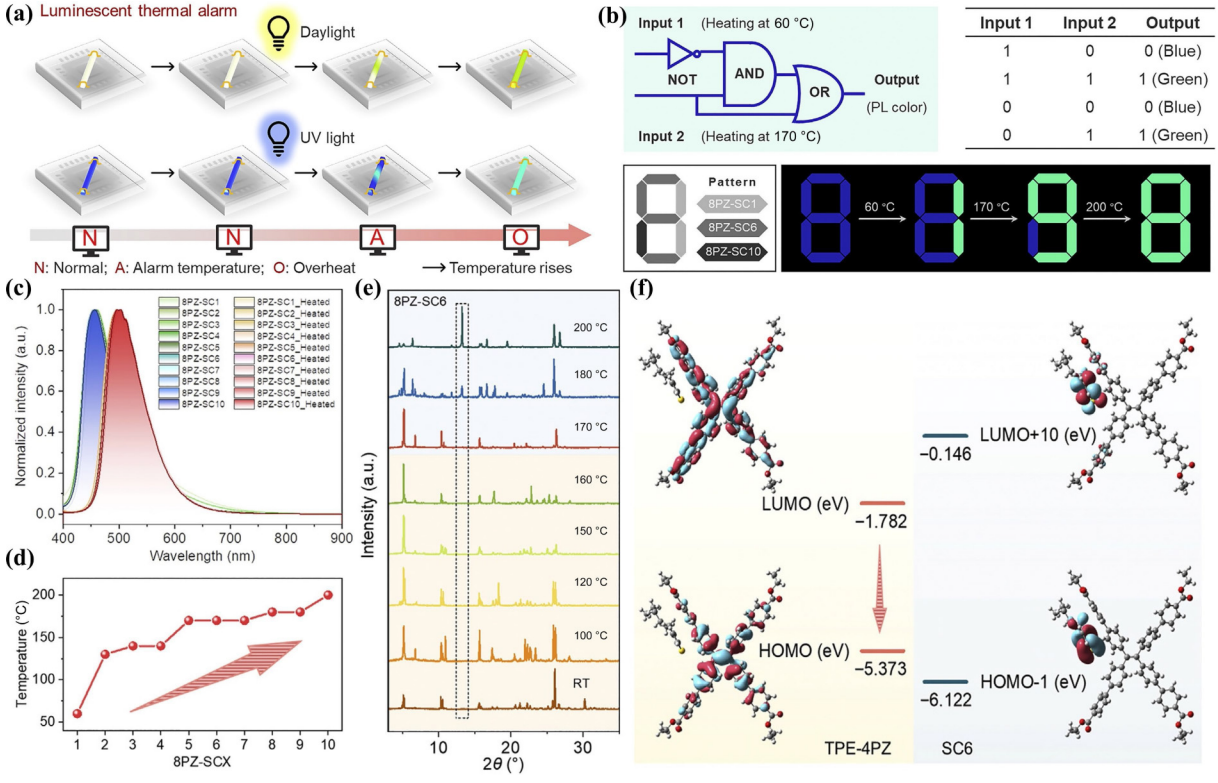


**Figure 15** (a) Schematic of 8PZ-SCX cocrystals used as luminescent temperature alarms. (b) A two-input combinational (a combination of NOT, AND, and OR logic functions) logic gate. Input 1 and input 2 represent heating at 60 and 170 °C, respectively, and output is the luminescence color. (c) Emission spectra of the host–guest cocrystals of 8PZ-SCX and their emission spectra after structural transformations (excited at 365 nm). (d) Alarm temperatures of 8PZ-SCX cocrystals. (e) Temperature-dependent PXPD patterns of 8PZ-SC6. (f) TD-DFT-calculated molecular energy levels based on the cocrystal structure of 8PZ-SC6. Reproduced with permission from Ref. [110], © Elsevier Inc. 2023.

elastic pressure-acoustic bimodal sensors, denoted as HOF-TTA@MF (1 and 2) (Fig. 16(a)) by integrating a blue-emitting HOF-TTA as a luminophore with melamine foam (MF). During the luminescent pressure sensing process, sensor 1 demonstrated outstanding characteristics, including maximum sensitivity (132.02 $kPa^{-1}$), a low minimum detection limit (0.01333 Pa), rapid response time (20 ms), high precision, and excellent recyclability. Sensor 2, serving as a luminescent auditory sensor, displayed the highest response to sound at 520 Hz within the frequency range of 255–1453 Hz. Specifically, when sensing sound at 520 Hz, sensor 2 exhibited high sensitivity (1,648,441.3 $cps{\cdot}Pa^{-1}{\cdot}cm^{-2}$), a low detection limit (0.36 dB), and an ultrafast response time (10 ms) within the sound range of 11.47–91.77 dB. The sensing mechanisms for pressure and auditory stimuli have been comprehensively analyzed using finite element simulation. Moreover, sensors 1 and 2, as human–machine interactive bimodal sensors (Fig. 16(b)), exhibited the ability to recognize nine different objects accurately and robustly, as well as the word information of "Health", "Phone", and "Tong Ji". This study presented a straightforward fabrication method for a luminescent pressure-auditory bimodal sensor based on HOF (TTA). Additionally, it introduced new recognition functions and expanded the capabilities of bifunctional sensors.

**Synergistic photo- and chemo-responses.** Photo-responsive functional materials have become a popular area of research due to the excellent properties of light energy, such as being green, remote controllable, and transient. However, current research is primarily focused on single light-responsive systems, and developing multiple controllable light-responsive systems remains a challenge. An acid-sensitive porous HOF was constructed by Abderrazzak Douhal et al. [121] using hexaazanaphthylene derivatives with carboxyphenyl groups. Single-crystal X-ray diffraction analysis successfully determined the precise structures of the 1,2,4-trichlorobenzene solvate 1,2,4-trichlorobenzene solvate [CPHATN-1(TCB)] and the activated HOF with permanent pores (CPHATN-1a) (Fig. 17(a)). The crystals of the HOF exhibited rich photochemical properties attributed to intramolecular charge transfer and interunit proton transfer reactions. Femtosecond (fs) experiments on the crystal demonstrate that these events occurred within ≤ 200 fs and 1.2 ps, respectively (Fig. 17(b)). Moreover, single-crystal fluorescence microscopy revealed changes in the emission spectrum, likely attributed to defects and highly anisotropic behavior, indicating an ordered crystal structure with a preferential orientation of molecular dipole moments. CPHATN-1a was notably characterized by a reversible color change from yellow to reddish-brown induced by vapor acid, attributed to the protonation of the pyridinyl nitrogen atom embedded in its π-conjugated core. Moreover, the emission of CPHATN-1a can be switched on/off.

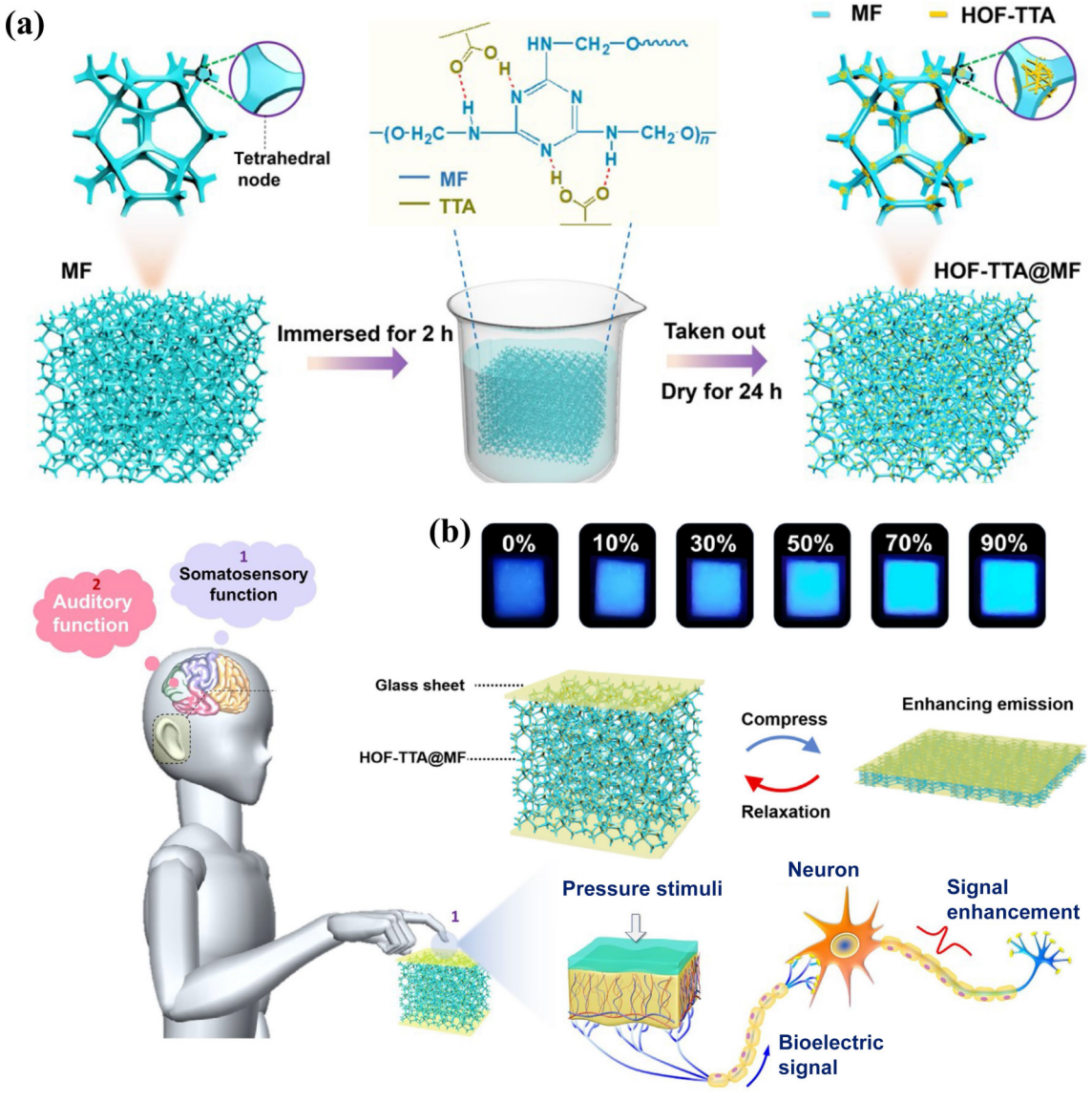


**Figure 16** (a) Schematic diagram of the preparation process of HOF-TTA@MF. (b) Compress-relaxation process and luminescent pictures upon 0%–90% pressing strain of 1. Reproduced with permission from Ref. [120], © Wiley-VCH GmbH 2023.

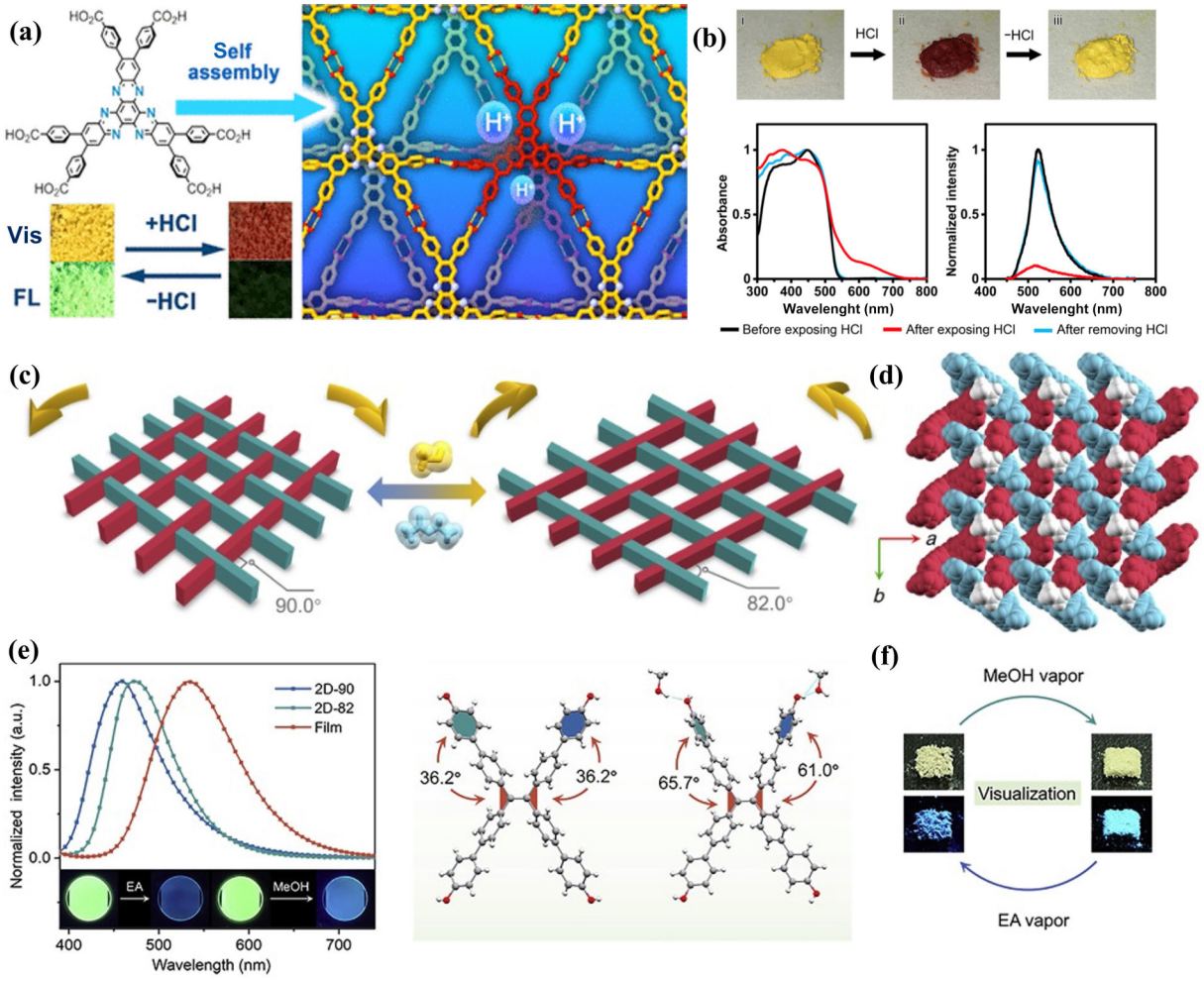


**Figure 17** (a) HCl-responsive color changes of crystalline bulk of CPHATN-1a, (b) The crystalline bulk of CPHATN-1a before exposure, after 37%-HCl was dropped on, and after heating at 423 K for 30 min. The absorption and emission spectra of solid CPHATN-1a upon exposing to HCl atmosphere for 40 min and after leaving the exposed crystals in the air for 48 h to remove HCl. Reproduced with permission from Ref. [121], © American Chemical Society 2019. (c) Illustration of reversible structural transformations between 2D-90 and 2D-82. Atoms of MeOH and EA molecules are colored yellow and light blue, respectively, for clarity. (d) SXRD structure of 2D-83. Atoms of TPE-4PhOH molecules in strands arranged in different directions are colored light blue and red, and atoms of EtOH molecules are colored white for clarity. (e) Distribution of intermolecular NCI regions at entanglement locations of the single-crystal structures of 2D-90 (left) and 2D-82 (right). (f) the visualization of reversible structural transformations by dynamic luminescence behaviors. Upper: images under daylight. Lower: images under 365 nm UV light. Reproduced with permission from Ref. [116], © Elsevier Inc. 2021.

In 2021, Chi et al. [116] demonstrated a dynamic 2D woven HOF with permanent porosity constructed through the interlocking of 1D strands. The 1D strands with holes were assembled by O–H···O hydrogen bonds with the changeful feature, into which X-shaped organic building blocks of orthogonal 1D strands can be interlocked. Due to the existence of the changeful hydrogen bonds, the angle between warps and wefts can be switched between 90.0° and 82.0° when responding to ethyl acetate (EA) and methanol (MeOH) vapors (Figs. 17(c), 17(e), and 17(f)), respectively, revealing the exceptional dynamics of the molecular woven structure. During the reversible structural transformations, the woven HOF also exhibited large-scale elasticity switching and high-contrast stimuli-responsive luminescence behaviors.

## 4 Electro-responses

### 4.1 Electrocatalysis with HOFs

Despite the growing research interest in HOFs, their potential in electrochemical applications was limited by the weak nature of the hydrogen bonds, which are susceptible to dissociation in the solution, compromising the structural integrity of HOFs [122].

In 2021, Wang et al. demonstrated that the solution stability of HOFs may be improved by designing and introducing multisite hydrogen bonding within HOFs (Fig. 18(a)) [123]. Using this strategy, 2D molecular sheets were prepared from diamino triazole linkers for the first time. This solution-stable HOF exhibited an excellent electrochemical performance for $Na^+$ ion storage (Fig. 18(b)). It enabled an exceptional cycle life of > 10,000 cycles at 1 $A{\cdot}g^{-1}$, which is far superior to most other organic electrode materials (Figs. 18(c) and 18(d)). Theoretical simulations indicated that the activation barrier for the intralayer or interlayer diffusion of $Na^+$ within the organic frameworks was small.

Recently, to study the selective two-electron redox reactions in acidic media, we screened 32 different metalloporphyrin 2-e-oxygen reduction reactions (ORRs) against $H_2O_2$ using high-throughput density flooding calculations [124]. Among them, cobalt porphyrins have the best activity and selectivity with theoretical overpotentials as low as 0.04 V. Guided by the theoretical predictions, we prepared hydrogen-bonded cobalt porphyrin skeletons through the self-assembly of TCPP-Co in solution. PFC-72-Co was characterized by high structural crystallinity, large specific surface area, and abundant catalytic centers. This HOF can efficiently and consistently produce $H_2O_2$ in 0.1 M $HClO_4$ with an onset potential of 0.68 V. The $H_2O_2$ selectivity is > 90% within a wide potential window. The TOF value of 10.9 $s^{-1}$ at 0.55 V is not only much better than that of

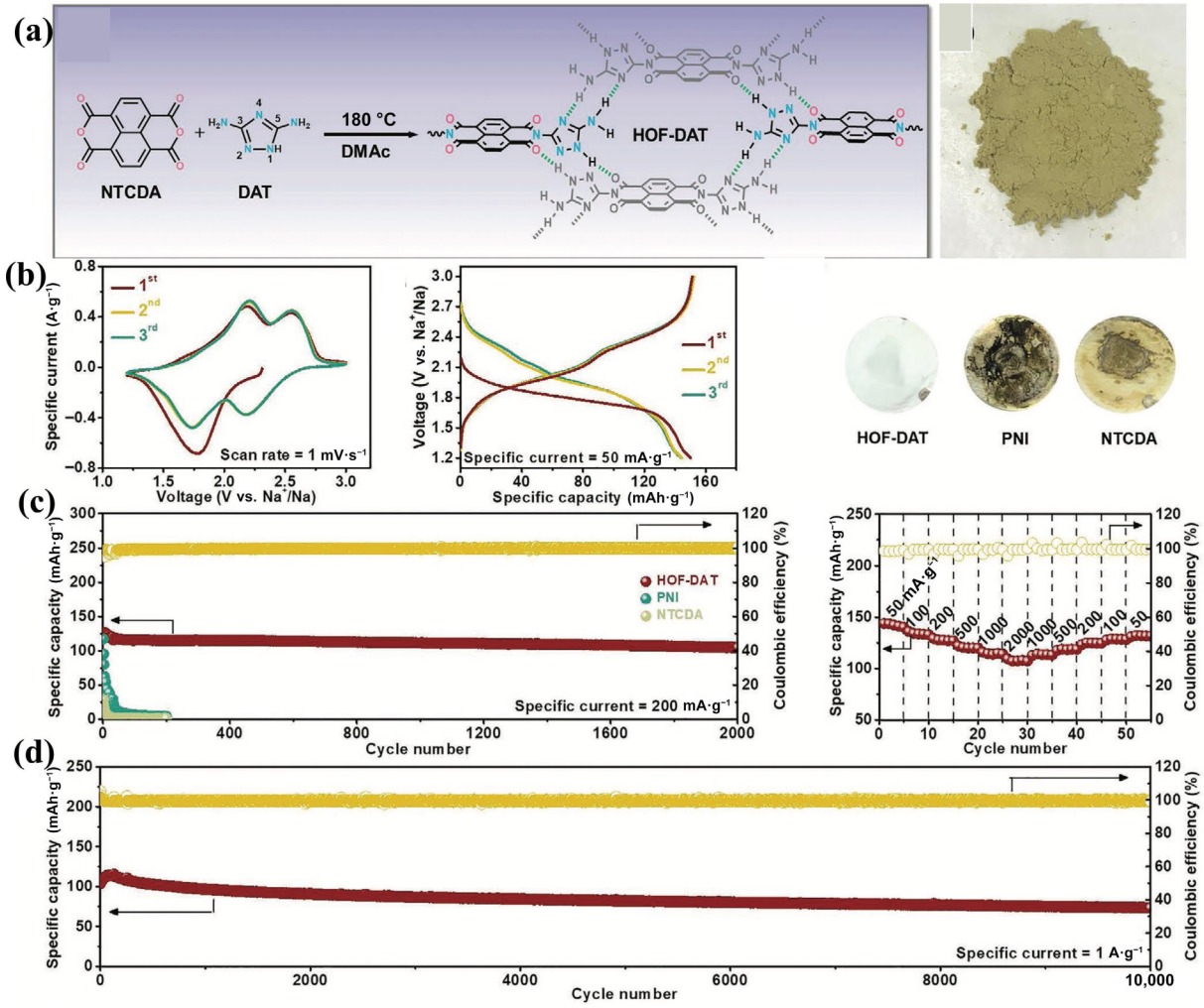


**Figure 18** (a) Schematic synthesis of HOF-DAT. (b) Photograph of HOFDAT powders. (c) CV curves of HOF-DAT at 1 mV·s$^{-1}$. (d) Galvanostatic charge and discharge curves of HOF-DAT for the first 3 cycles at 50 mA·g$^{-1}$. (e) Cycling stability of HOF-DAT, NTCDA or PNI at 200 mA·g$^{-1}$. (f) Separator membranes of HOF-DAT, NTCDA or PNI after 10 cycles. (g) Rate capability of HOF-DAT. (h) cycling stability of HOF-DAT at 1 A·g$^{-1}$. Reproduced with permission from Ref. [123], © Wiley-VCH GmbH 2021.

organic or inorganic alloys, but it is also better than the state-of-the-art Pt/Pd-Hg alloy.

### 4.2 Electrochromic materials incorporating HOFs

Electrochromic (EC) materials are [125, 126] derived from metal oxides [127, 128], Violagen and its analogs [129], MOFs, and COFs [130], which have a wide range of applications in bright windows, information storage, electronic displays, dynamic mirrors, etc. The unique properties of HOFs, such as easy modification, adjustable structure, and high porosity, can help achieve the regulation of electrochromism at the atomic level. These characteristics can speed up the electron transmission rate, improving electronic transmission performance. Therefore, HOFs have good prospects in the field of electrochromism.

HOFs can form charged particles during protonation or deprotonation due to the extensive presence of proton and hydrogen donor/acceptor sites in the structure, which inspired us to apply electrophoresis deposition (EPD) to prepare HOF films. In 2020, using the EPD method, we successfully deposited a high porosity HOF, PFC-1, on transparent fluorine-doped tin oxide (FTO) glass as the electrochromic bright window (Fig. 19(a) and 19(b)) [131]. The resulting film had a uniform morphology, dense surface, and high crystallinity, and the method was equally applicable to other HOFs and substrates. The PFC-1 films prepared on FTO glass had reversible electrochromic properties, with the color changing from yellow to blue-violet and the transmittance decreasing from 75% to 25%. In addition, due to the presence of unbound carboxylic acids at structural defects and particle surfaces, the films can be further modified with Fe ions to achieve multi-state electrochromic, demonstrating the unique tunability of HOF for specific needs. We then used an efficient and low-cost electrostatic spray deposition (ESD) method to directly prepare large-area HOF films (30 cm × 30 cm) on unmodulated conductive substrates (Fig. 19(d)). Combining the ESD with a templating method, HOF membranes can be easily fabricated in various patterns, including deer-shaped and horse-shaped membranes (Fig. 19(f)). The obtained film had excellent electrochromic properties, achieved multi-color changes from yellow to green and purple, and can be dual-band tuned at 550 and 830 nm. PFC-1 films can change color quickly (within 10 s) thanks to the inherent channels of the HOF and the additional film porosity created by ESD [132]. Furthermore, we constructed large-area patterned electrochromic devices based on the above films to demonstrate their potential for practical applications.

## 5 Photoelectric synergistic response

In recent years, photoelectrochemical (PEC) detection has emerged as an innovative biosensing technique widely employed for trace analysis due to its ultrahigh sensitivity, low background noise, and good reproducibility compared to traditional detection methods [133]. In a typical detection process, the photoactive material serves as both a functional layer for photoelectron generation and an identification layer for the analyte. Unlike

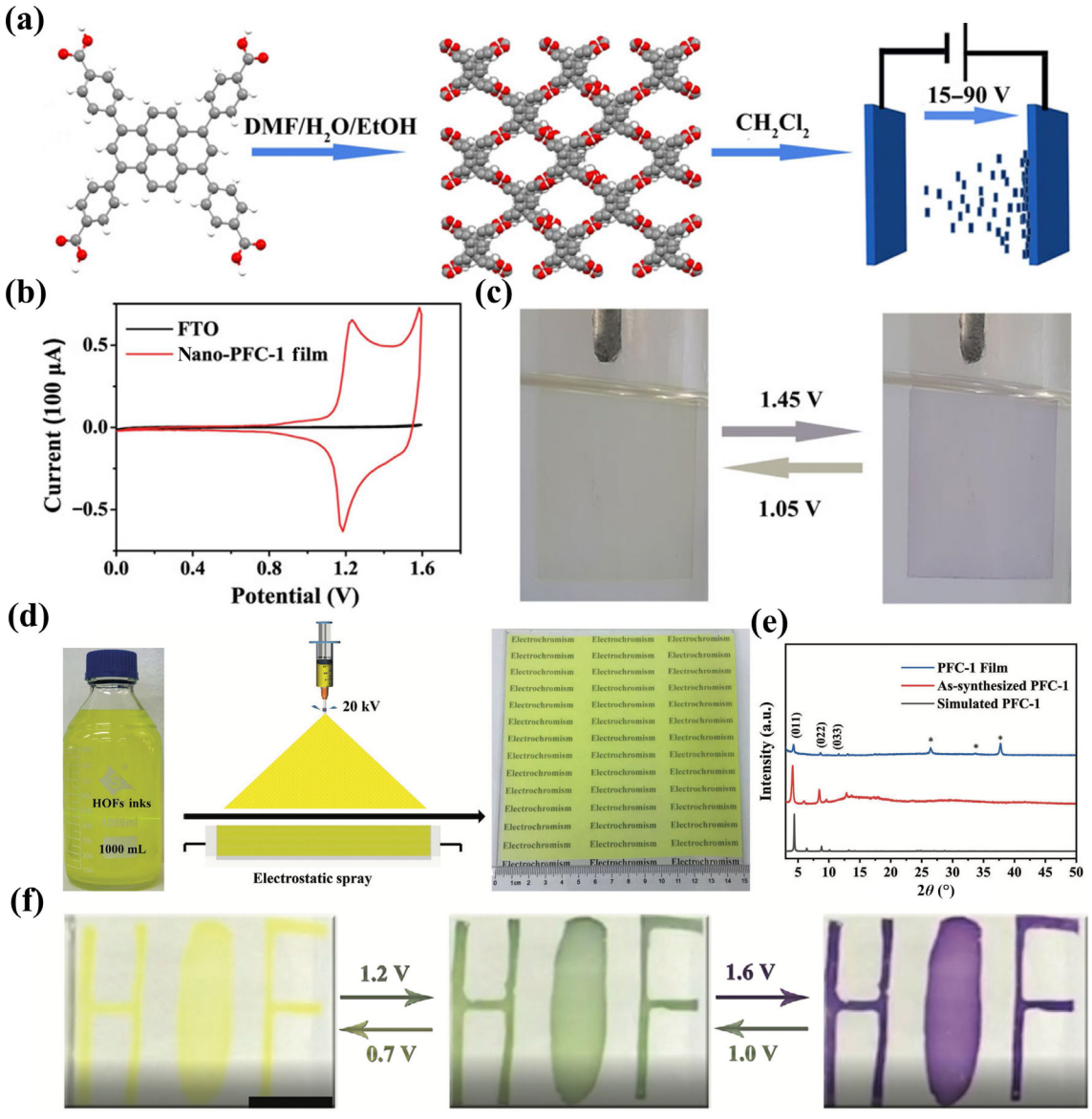


**Figure 19** (a) Fabrication of the nano-PFC-1 film by EPD (C gray, H, white, O red). (b) CV curves of the nano-PFC-1 film and bare FTO substrate at a scan rate of 5 mVs. (c) Photographs of the nano-PFC-1 EC film with applied potentials of 1.45 and 1.05 V during CV cycles (vs. Ag/AgCl). Reproduced with permission from Ref. [131], © Wiley-VCH GmbH 2020. (d) The schematic of preparation of PFC-1 HOF film via an electrostatic deposition method. (e) The powdered X-ray diffraction (PXRD) patterns of simulated PFC-1 (black), as-synthesized PFC-1 powder (red), and PFC-1 film (blue). The peaks highlighted by * are attributed to those of FTO substrates. (f) Images of the patterned PFC-1 film during the CV process between 0 and 1.8 V (vs $Ag^+/Ag$) showing clear color changes: HOF pattern and deer pattern. Scale bar: 2 cm. Reproduced with permission from Ref. [132], © Wiley-VCH GmbH 2023.

transition metal-based photoelectric semiconductor materials, such as ZnO and $Cu_2O$, which only provide surface chemical recognition, analogous HOF-based photoelectric sensors offer additional sensing capabilities due to their inherent porosity. Furthermore, the photoactivity, semi-conductivity, and ordered nanopores of porous molecular traps can facilitate photo-induced electron generation and transport and serve as both a size and site recognition layer, enabling selective detection of target analytes in the presence of interfering substances [133].

In 2022, Xiao et al. [134] utilized aggregation-induced enhanced emission (AIEE)-active $H_4$TBAPy as a building block to synthesize a novel HOF-based electrochemiluminescence (ECL) material called Py-HOF (Fig. 20(b)). They introduced a pyrene-based hydrogen-bonded organic framework (Py-HOF) with outstanding ECL performance, which was prepared by using 1,3,6,8-tetrakis (p-benzoic acid) pyrene ($H_4$TBAPy) with an AIEE property as the building block, and exhibited a stronger ECL emission than that of the $H_4$TBAPy monomer. $H_4$TBAPy aggregates, the low-porosity Py-HOF-210 °C and Py-HOF-180 °C. We have coined the term "the porosity and aggregation-induced enhanced ECL (PAIE-ECL)" for this intriguing phenomenon. The Py-HOF displayed superb and stable ECL intensity, not only because the luminophore $H_4$TBAPy was assembled into the Py-HOF via four pairs of O–H···O hydrogen bonds, which constrained the intramolecular movements to reduce nonradiative transition, but also because the $H_4$TBAPy in Py-HOF was stacked in a slipped face-to-face mode to form J-aggregates that benefited the ECL enhancement. Additionally, the high porosity of Py-HOF enabled the rapid transfer of ions, electrons, and co-reactants, enhancing the utilization of luminophores. Due to its excellent ECL properties, Py-HOF served as an ECL probe. It was integrated with a 3D DNA nanomachine amplification strategy to fabricate a "switch" ECL sensor, enabling ultra-sensitive detection of miRNA-141 (Fig. 20(a)).

In 2022, Li et al successfully encapsulated ultrafine sub-1 nm AgNPs within HOFs using an environmentally friendly photoreduction synthesis method conducted under ambient conditions without needing harmful chemicals, stringent conditions, or cumbersome operations (Fig. 20(c)) [135]. These AgNPs@HOFs demonstrated not only enhanced photocurrent

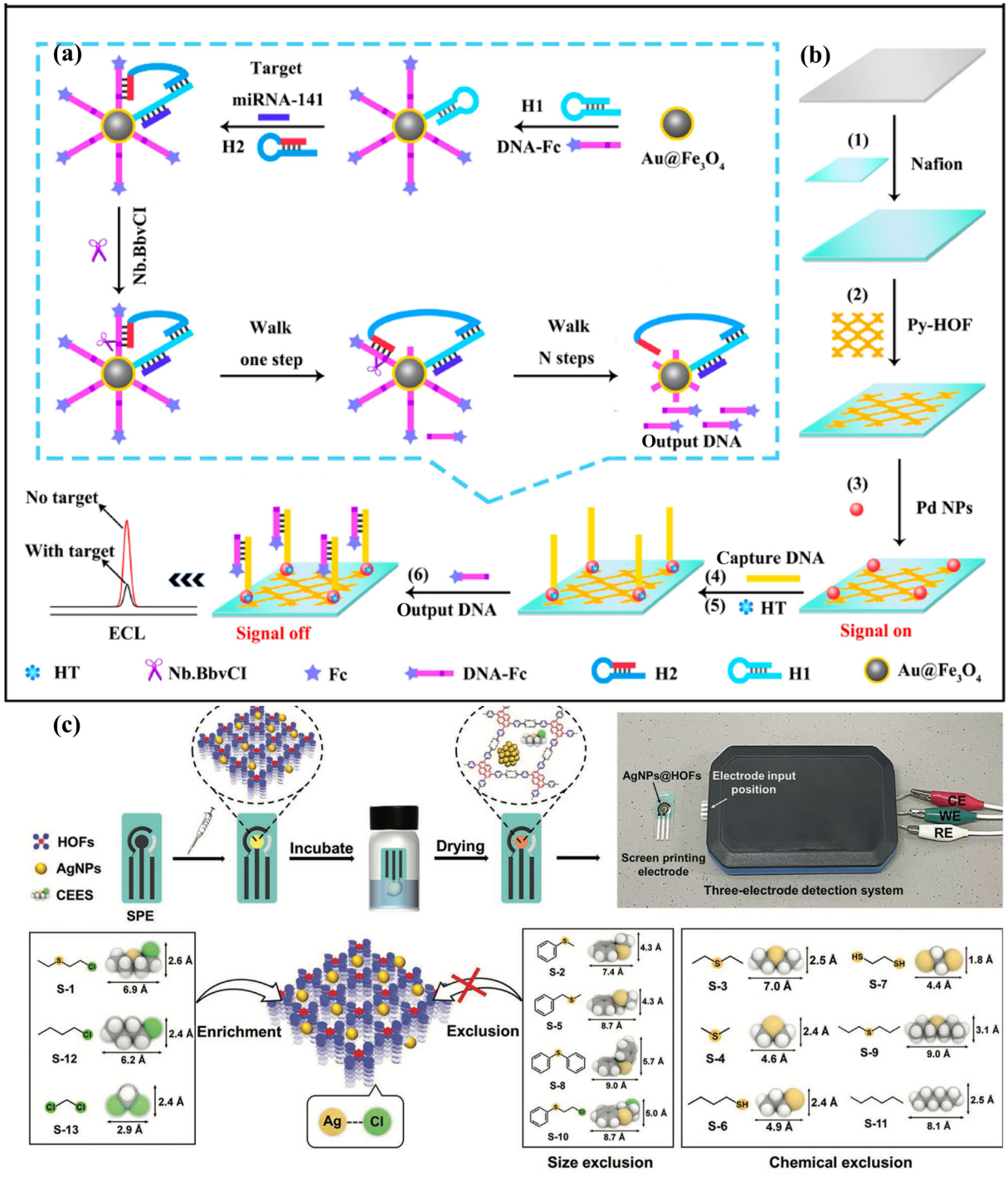


**Figure 20** (a) Fabrication of the ECL sensor; (b) 3D DNA nanomachine amplification strategy. Reproduced with permission from Ref. [134], © American Chemical Society 2022. (c) Scheme of HOF-101 detecting nine simulants. Reproduced with permission from Ref. [135], © Wiley-VCH GmbH 2022.

compared to pristine HOFs, selected MOFs, and semiconductors, but they can also selectively enrich mustard gas mimics through the size exclusion effect. The photo-electrochemistry (PEC) sensor demonstrated a distinct photocurrent response to 13 diverse mustard gas mimics. The combined size exclusion effect and specific recognition of Ag(I) and –Cl on these mimics contributed to the high selectivity of the AgNPs@HOF-modified PEC sensor, which achieved a CEES detection limit of 15.8 nmol·L$^{-1}$ and encompassed a broad linear range from 20 to 400 nmol·L$^{-1}$. The straightforward preparation method described in this study could be employed to obtain other types of metal nanoparticles (e.g., Au, Pt, Pd NPs) encapsulated within HOFs, thereby paving the way for the advancement of highly selective, sensitive, and portable detection devices based on PEC sensing for various toxic chemical warfare agents (CWAs) like mustard gas and nerve agents.

Recently, a facile bottom-up growth method was also reported to achieve a high yield (89%) of large-area (up to 23,500 μm$^2$) porphyrin tablets with controllable thicknesses ranging from 0.298 to 2.407 μm [136]. The tablets exhibited a high density of 2D hydrogen bonding in their structure. The DAT moieties on the porphyrin molecules facilitated the formation of complementary hydrogen bonds between the structures and acted as recognition sites for the selective adsorption of $CO_2$ in the resulting porous HOF materials. FDU-HOF-2 can be grown and deposited directly onto various substrates, such as silica, carbon, and metal oxides, through *in situ* self-assembly in formic acid (Fig. 21(a)). As proof of concept, we fabricated label-free PEC sensors for $CO_2$ detection by depositing FDU-HOF-2 onto screen-printed electrodes (Fig. 21(g)). The resulting PEC sensor operated in a signal-off mode, demonstrating a low $CO_2$ detection limit of 2.3 ppm, reusability

for at least 30 cycles, and long-term operational stability lasting at least 30 days.

## 6 Conclusion and perspective

In this review, we provided an overview of recent research progress made toward developing stable HOFs, focusing on five prominent synthetic strategies: (1) π–π stacking, (2) interpenetration, (3) chemical crosslinking, (4) charge-assisted H-bonds, and (5) mechanical synthesis. A large number of stable HOFs with diverse structures have been synthesized using these strategies, and they have been studied for various applications. Despite the limited active sites in HOFs compared to MOFs, HOFs have many unique properties, such as their ability to recrystallize and self-repair, which can facilitate their recyclability and reduce material consumption. Additionally, the weaker intermolecular interaction forces between HOF building blocks give HOF the potential to be a responsive material to external stimuli. For example, by incorporating suitable motifs, HOFs can gain intrinsic photo-responsive abilities, and a suitable topology with π–π interactions can further facilitate the transmission of photocurrent. Moreover, the metal-free nature of HOFs makes them attractive materials for biomedical applications.

Thanks to the improved stability of HOFs and their unique properties, the function of HOFs has also been extended significantly over the past decade. Taking advantage of the photoactivities and photo-responses of stable HOFs, researchers have utilized HOFs for photocatalysis, photocatalytic hydrogen production, and photodynamic and photothermal therapy. Some HOFs also demonstrated biomimetic photo-responsive enzymatic activities, or can change their color or electron/photon conductivity in response to external stimuli, expanding their applications in stimuli-responsive biocatalysis, photochromic devices, sensing, and others. In addition to stable HOFs with rigid structures, stable FHOFs with flexible structures have also been investigated. These FHOFs can undergo a reversible structural transformation in response to one or two external stimuli, enabling their synergistic response to photo- and one other external stimuli, including temperature, pressure, and chemical stimuli. Furthermore, by improving the stability of HOFs using the strategies mentioned above, HOFs have also found

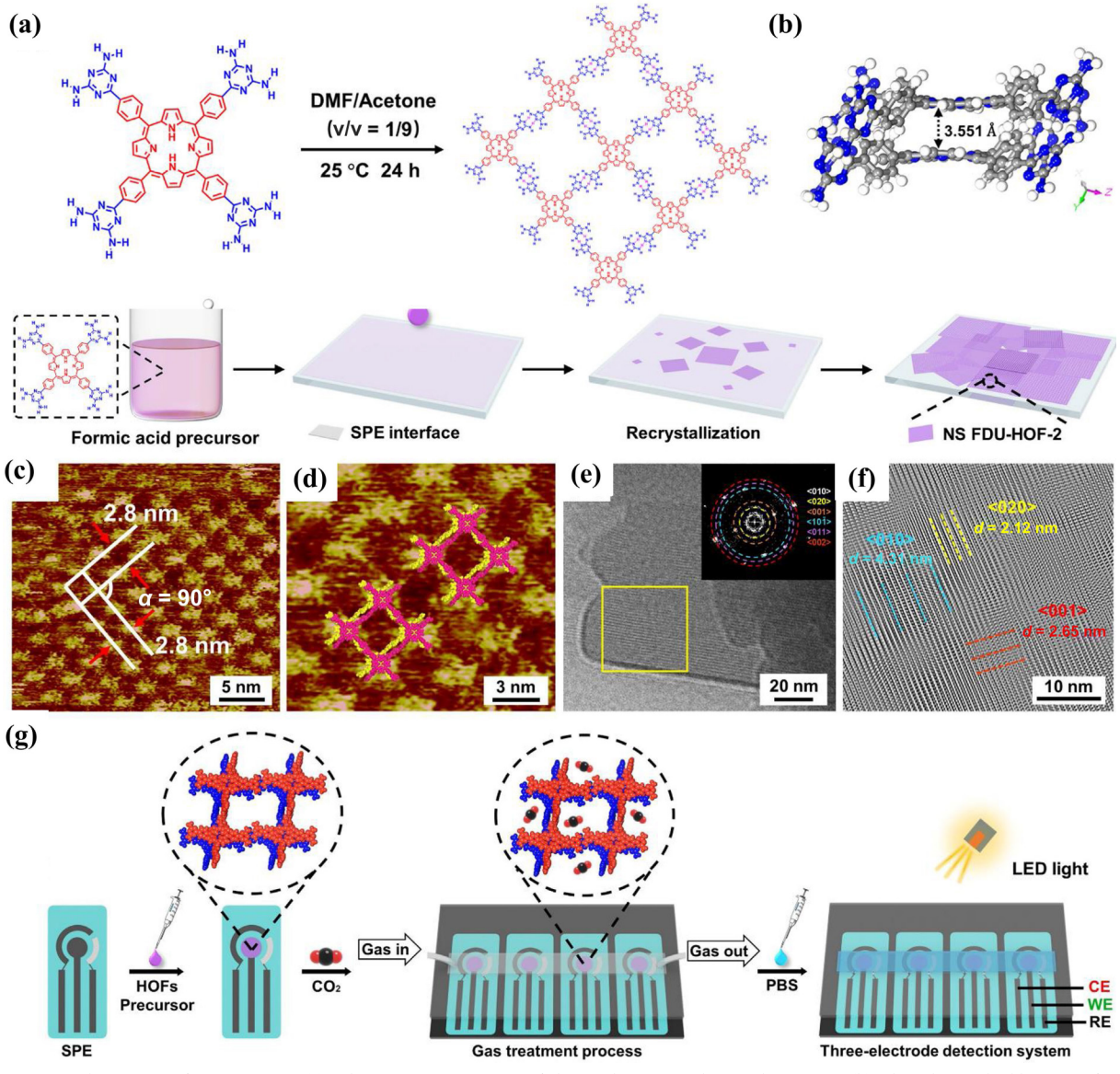


**Figure 21** Crystal structure of FDU-HOF-2. (a) Schematic representation of the synthesis procedure and structure. (b) The adjacent building unit from two independent networks forms multiple face-to-face π–π stacking at 3.551 Å. (c) and (d) Medium-scale and high-resolution STM of NS FDU-HOF-2 self-assembly structure at rt on 1-heptanoic acid /HOPG interface. (e) and (f) Structural profile of FDU-HOF-2 by low-electron-dose cryo-EM, and the FFT pattern of the selected area (inset) that assigned to FDU-HOF-2 crystal along the <010>, <020>, and <001> directions. (g) Scheme for fabricating the PEC sensor decorated with FDU-HOF-2 and process of $CO_2$ sensing. Reproduced with permission from Ref. [136], © Wiley-VCH GmbH 2023.

applications in electrocatalysis, electrochromic devices, and photoelectrochemical sensing.

The past decade has seen rapid and remarkable development in the HOF field, ranging from structure design and synthetic strategies to the expansion of their applications. This review demonstrated the great potential of HOFs as functional photo- and electro-responsive materials in various applications. However, most of the research involving HOFs is still in its infancy, which requires systematic investigation both experimentally and computationally to understand the structure–function relationships of these novel materials and their function mechanisms. Machine learning may be employed to accelerate the discovery and optimization of new HOF structures with desirable properties for targeted practical applications. Significant research efforts are still needed for this exciting research field to achieve its full potential.

## Acknowledgements

The authors thank the support from Chinese Academy of Sciences (No. JCTD-2022-12 CAS youth interdisciplinary team). Y. L. acknowledges the support from the National Science Foundation (No. HRD-2112554).

## References

[1] Lin, C. X.; Liu, Y.; Rinker, S.; Yan, H. DNA tile based self-assembly: Building complex nanoarchitectures. *Chemphyschem* **2006**, *7*, 1641–1647.

[2] Pfeifer, W.; Sacca, B. From nano to macro through hierarchical self-assembly: The DNA paradigm. *Chembiochem* **2016**, *17*, 1063–1080.

[3] Zhang, Y. Z.; Tu, J.; Wang, D. Q.; Zhu, H. T.; Maity, S. K.; Qu, X. M.; Bogaert, B.; Pei, H.; Zhang, H. B. Programmable and multifunctional DNA-based materials for biomedical applications. *Adv. Mater.* **2018**, *30*, 1703658.

[4] Hu, Y. Q.; Wang, Y.; Yan, J. H.; Wen, N. C.; Xiong, H. J.; Cai, S. D.; He, Q. Y.; Peng, D. M.; Liu, Z. B.; Liu, Y. F. Dynamic DNA assemblies in biomedical applications. *Adv. Sci.* **2020**, *7*, 2000557.

[5] Liu, B. T.; Gong, S. H.; Jiang, X. T.; Zhang, Y.; Wang, R.; Chen, Z. J.; Zhang, S.; Kirlikovali, K. O.; Liu, T. F.; Farha, O. K. et al. A solution processible single-crystal porous organic polymer. *Nat. Synth.* **2023**, *2*, 873–879.

[6] Abrahams, B. F.; Hoskins, B. F.; Liu, J. P.; Robson, R. The archetype for a new class of simple extended 3D honeycomb frameworks. The synthesis and X-ray crystal structures of $Cd(CN)_{5/3}(OH)\omega^1/3(C_6H_{12}N_4)$, $Cd(CN)r^{1/3}(C_6H_{12}N_4)$, and $Cd(CN)2^2/3H_2O{\cdot}tBuOH$ ($C_6H_{12}N_4$ = Hexamethylenetetramine) revealing two topologically equivalent but geometrically different frameworks. *J. Am. Chem. Soc.* **1991**, *113*, 3045–3051.

[7] Eddaoudi, M.; Moler, D. B.; Li, H. L.; Chen, B. L.; Reineke, T. M.; O'Keeffe, M.; Yaghi, O. M. Modular chemistry: Secondary building units as a basis for the design of highly porous and robust metal-organic carboxylate frameworks. *Acc. Chem. Res.* **2001**, *34*, 319–330.

[8] Li, H. L.; Thomas, M.; Groy, T. L.; Yaghi, O. M. Establishing microporosity in open metal-organic frameworks: Gas sorption isotherms for Zn(BDC) (BDC=1,4-benzenedicarboxylate). *J. Am. Chem. Soc.* **1998**, *120*, 8571–8572.

[9] Kim, J.; Chen, B. L.; Reineke, T. M.; Li, H. L.; Eddaoudi, M.; Moler, D. B.; O'Keeffe, M.; Yaghi, O. M. Assembly of metal-organic frameworks from large organic and inorganic secondary building units: New examples and simplifying principles for complex structures. *J. Am. Chem. Soc.* **2001**, *123*, 8239–8247.

[10] Kondo, M.; Yoshitomi, T.; Matsuzaka, H.; Kitagawa, S.; Seki, K. Three-dimensional framework with channeling cavities for small molecules: $\{[M_2(4,4'\text{-bpy})_3(NO_3)_4]{\cdot}xH_2O\}n$ (M = Co, Ni, Zn). *Angew. Chem., Int. Ed.* **1997**, *36*, 1725–1727.

[11] Li, H. L.; Eddaoudi, M.; O'Keeffe, M.; Yaghi, O. M. Design and synthesis of an exceptionally stable and highly porous metal-organic framework. *Nature* **1999**, *402*, 276–279.

[12] O'Keeffe, M. Design of MOFs and intellectual content in reticular chemistry: A personal view. *Chem. Soc. Rev.* **2009**, *38*, 1215–1217.

[13] O'Keeffe, M.; Peskov, M. A.; Ramsden, S. J.; Yaghi, O. M. The reticular chemistry structure resource (RCSR) database of, and symbols for, crystal nets. *Acc. Chem. Res.* **2008**, *41*, 1782–1789.

[14] Ockwig, N. W.; Delgado-Friedrichs, O.; O'Keeffe, M.; Yaghi, O. M. Reticular chemistry: Occurrence and taxonomy of nets and grammar for the design of frameworks. *Acc. Chem. Res.* **2005**, *38*, 176–182.

[15] Hoskins, B. F.; Robson, R. Design and construction of a new class of scaffolding-like materials comprising infinite polymeric frameworks of 3D-linked molecular rods. A reappraisal of the $Zn(CN)_2$ and $Cd(CN)_2$ structures and the synthesis and structure of the diamond-related frameworks $[N(CH_3)_4][Cu^{I}Zn^{II}(CN)_4]$ and $Cu^{I}$[4,4′,4″,4‴-tetracyanotetraphenylmethane]$BF_4{\cdot}xC_6H_5NO_2$. *J. Am. Chem. Soc.* **1990**, *112*, 1546–1554.

[16] Brunet, P.; Demers, E.; Maris, T.; Enright, G. D.; Wuest, J. D. Designing permeable molecular crystals that react with external agents to give crystalline products. *Angew. Chem., Int. Ed.* **2003**, *42*, 5303–5306.

[17] Furukawa, H.; Cordova, K. E.; O'Keeffe, M.; Yaghi, O. M. The chemistry and applications of metal-organic frameworks. *Science* **2013**, *341*, 1230444.

[18] Kolotuchin, S. V.; Fenlon, E. E.; Wilson, S. R.; Loweth, C. J.; Zimmerman, S. C. Self-assembly of 1,3,5-benzenetricarboxylic acids (trimesic acids) and several analogues in the solid state. *Angew. Chem., Int. Ed.* **1996**, *34*, 2654–2657.

[19] Li, B.; Wen, H. M.; Cui, Y. J.; Zhou, W.; Qian, G. D.; Chen, B. L. Emerging multifunctional metal-organic framework materials. *Adv. Mater.* **2016**, *28*, 8819–8860.

[20] Little, M. A.; Cooper, A. I. The chemistry of porous organic molecular materials. *Adv. Funct. Mater.* **2020**, *30*, 1909842.

[21] Malek, N.; Maris, T.; Perron, M. È.; Wuest, J. D. Molecular tectonics: Porous cleavable networks constructed by dipole-directed stacking of hydrogen-bonded sheets. *Angew. Chem., Int. Ed.* **2005**, *44*, 4021–4025.

[22] Wuest, J. D. Atoms and the void: Modular construction of ordered porous solids. *Nat. Commun.* **2020**, *11*, 4652.

[23] Zhou, H. C.; Long, J. R.; Yaghi, O. M. Introduction to metal-organic frameworks. *Chem. Rev.* **2012**, *112*, 673–674.

[24] He, Y. B.; Xiang, S. C.; Chen, B. L. A microporous hydrogen-bonded organic framework for highly selective $C_2H_2/C_2H_4$ separation at ambient temperature. *J. Am. Chem. Soc.* **2011**, *133*, 14570–14573.

[25] Yin, Q.; Zhao, P.; Sa, R. J.; Chen, G. C.; Lü, J.; Liu, T. F.; Cao, R. An ultra-robust and crystalline redeemable hydrogen-bonded organic framework for synergistic chemo-photodynamic therapy. *Angew. Chem., Int. Ed.* **2018**, *57*, 7691–7696.

[26] Bao, Z. B.; Xie, D. Y.; Chang, G. G.; Wu, H.; Li, L. Y.; Zhou, W.; Wang, H. L.; Zhang, Z. G.; Xing, H. B.; Yang, Q. W. et al. Fine tuning and specific binding sites with a porous hydrogen-bonded metal-complex framework for gas selective separations. *J. Am. Chem. Soc.* **2018**, *140*, 4596–4603.

[27] Hu, F.; Liu, C. P.; Wu, M. Y.; Pang, J. D.; Jiang, F. L.; Yuan, D. Q.; Hong, M. C. An ultrastable and easily regenerated hydrogen-bonded organic molecular framework with permanent porosity. *Angew. Chem., Int. Ed.* **2017**, *56*, 2101–2104.

[28] Nandi, S.; Chakraborty, D.; Vaidhyanathan, R. A permanently porous single molecule H-bonded organic framework for selective $CO_2$ capture. *Chem. Commun.* **2016**, *52*, 7249–7252.

[29] Wang, B.; Lv, X. L.; Lv, J.; Ma, L.; Lin, R. B.; Cui, H.; Zhang, J.; Zhang, Z. J.; Xiang, S. C.; Chen, B. L. A novel mesoporous hydrogen-bonded organic framework with high porosity and stability. *Chem. Commun.* **2019**, *56*, 66–69.

[30] Wang, L.; Yang, L. X.; Gong, L. L.; Krishna, R.; Gao, Z.; Tao, Y.; Yin, W. H.; Xu, Z. Z.; Luo, F. Constructing redox-active microporous hydrogen-bonded organic framework by imide-functionalization: Photochromism, electrochromism, and selective adsorption of $C_2H_2$ over $CO_2$. *Chem. Eng. J.* **2020**, *383*, 123117.

[31] Xi, X. J.; Li, Y.; Lang, F. F.; Xu, L.; Pang, J. D.; Bu, X. H. Robust porous hydrogen-bonded organic frameworks: Synthesis and applications in gas adsorption and separation. *Giant* **2023**, *16*, 100181.

[32] Yin, Q.; Li, Y. L.; Li, L.; Lü, J.; Liu, T. F.; Cao, R. Novel hierarchical meso-microporous hydrogen-bonded organic framework for selective separation of acetylene and ethylene versus methane. *ACS Appl. Mater. Interfaces* **2019**, *11*, 17823–17827.

[33] Yin, Q.; Lü, J.; Li, H. F.; Liu, T. F.; Cao, R. Robust microporous porphyrin-based hydrogen-bonded organic framework for highly selective separation of $C_2$ hydrocarbons versus methane. *Cryst. Growth Des.* **2019**, *19*, 4157–4161.

[34] Zentner, C. A.; Lai, H. W. H.; Greenfield, J. T.; Wiscons, R. A.; Zeller, M.; Campana, C. F.; Talu, O.; FitzGerald, S. A.; Rowsell, J. L. High surface area and *Z*′ in a thermally stable 8-fold polycatenated hydrogen-bonded framework. *Chem. Commun.* **2015**, *51*, 11642–11645.

[35] Zhang, X.; Li, L. B.; Wang, J. X.; Wen, H. M.; Krishna, R.; Wu, H.; Zhou, W.; Chen, Z. N.; Li, B.; Qian, G. D. et al. Selective ethane/ethylene separation in a robust microporous hydrogen-bonded organic framework. *J. Am. Chem. Soc.* **2020**, *142*, 633–640.

[36] Li, P.; He, Y. B.; Zhao, Y. F.; Weng, L. H.; Wang, H. L.; Krishna, R.; Wu, H.; Zhou, W.; O'Keeffe, M.; Han, Y. et al. A rod-packing microporous hydrogen-bonded organic framework for highly selective separation of $C_2H_2/CO_2$ at room temperature. *Angew. Chem., Int. Ed.* **2015**, *54*, 574–577.

[37] Li, P.; He, Y. B.; Arman, H. D.; Krishna, R.; Wang, H. L.; Weng, L. H.; Chen, B. A microporous six-fold interpenetrated hydrogen-bonded organic framework for highly selective separation of $C_2H_4/C_2H_6$. *Chem. Commun.* **2014**, *50*, 13081–13084.

[38] Wang, H. L.; Li, B.; Wu, H.; Hu, T. L.; Yao, Z. Z.; Zhou, W.; Xiang, S. C.; Chen, B. L. A flexible microporous hydrogen-bonded organic framework for gas sorption and separation. *J. Am. Chem. Soc.* **2015**, *137*, 9963–9970.

[39] Yang, W.; Yang, F.; Hu, T. L.; King, S. C.; Wang, H. L.; Wu, H.; Zhou, W.; Li, J. R.; Arman, H. D.; Chen, B. L. Microporous diaminotriazine-decorated porphyrin-based hydrogen-bonded organic framework: Permanent porosity and proton conduction. *Cryst. Growth Des.* **2016**, *16*, 5831–5835.

[40] Yang, W.; Li, B.; Wang, H. L.; Alduhaish, O.; Alfooty, K.; Zayed, M. A.; Li, P.; Arman, H. D.; Chen, B. L. A microporous porphyrin-based hydrogen-bonded organic framework for gas separation. *Cryst. Growth Des.* **2015**, *15*, 2000–2004.

[41] Wang, H. L.; Wu, H.; Kan, J. L.; Chang, G. G.; Yao, Z. Z.; Li, B.; Zhou, W.; Xiang, S. C.; Zhao, J. C. G.; Chen, B. L. A microporous hydrogen-bonded organic framework with amine sites for selective recognition of small molecules. *J. Mater. Chem. A* **2017**, *5*, 8292–8296.

[42] Wang, H. L.; Bao, Z. B.; Wu, H.; Lin, R. B.; Zhou, W.; Hu, T. L.; Li, B.; Zhao, J. C. G.; Chen, B. L. Two solvent-induced porous hydrogen-bonded organic frameworks: Solvent effects on structures and functionalities. *Chem. Commun.* **2017**, *53*, 11150–11153.

[43] Feng, S.; Shang, Y. X.; Wang, Z. K.; Kang, Z. X.; Wang, R. M.; Jiang, J. Z.; Fan, L. L.; Fan, W. D.; Liu, Z. N.; Kong, G. D. et al. Fabrication of a hydrogen-bonded organic framework membrane through solution processing for pressure-regulated gas separation. *Angew. Chem., Int. Ed.* **2020**, *59*, 3840–3845.

[44] Chen, T. H.; Popov, I.; Kaveevivitchai, W.; Chuang, Y. C.; Chen, Y. S.; Daugulis, O.; Jacobson, A. J.; Miljanić, O. S. Thermally robust and porous noncovalent organic framework with high affinity for fluorocarbons and CFCs. *Nat. Commun.* **2014**, *5*, 5131.

[45] Lü, J.; Perez-Krap, C.; Suyetin, M.; Alsmail, N. H.; Yan, Y.; Yang, S. H.; Lewis, W.; Bichoutskaia, E.; Tang, C. C.; Blake, A. J. et al. A robust binary supramolecular organic framework (SOF) with high $CO_2$ adsorption and selectivity. *J. Am. Chem. Soc.* **2014**, *136*, 12828–12831.

[46] Liao, M. S.; Scheiner, S. Electronic structure and bonding in metal porphyrins, metal = Fe, Co, Ni, Cu, Zn. *J. Chem. Phys.* **2002**, *117*, 205–219.

[47] Chen, X.; Takahashi, K.; Kokado, K.; Nakamura, T.; Hisaki, I. A proton conductive hydrogen-bonded framework incorporating 18-crown-6-ether and dicarboxy-*o*-terphenyl moieties. *Mater. Adv.* **2021**, *2*, 5639–5644.

[48] Delmas, L. C.; Horton, P. N.; White, A. J. P.; Coles, S. J.; Lickiss, P. D.; Davies, R. P. Siloxane-based linkers in the construction of hydrogen bonded assemblies and porous 3D MOFs. *Chem. Commun.* **2017**, *53*, 12524–12527.

[49] Guo, G. M.; Wang, D. B.; Zheng, X. H.; Bi, X. W.; Liu, S. P.; Sun, L. S.; Zhao, Y. J. Construction of tetraphenylethylene-based fluorescent hydrogen-bonded organic frameworks for detection of explosives. *Dyes Pigments.* **2022**, *197*, 109881.

[50] Hisaki, I.; Suzuki, Y.; Gomez, E.; Cohen, B.; Tohnai, N.; Douhal, A. Docking strategy to construct thermostable, single-crystalline, hydrogen-bonded organic framework with high surface area. *Angew. Chem., Int. Ed.* **2018**, *57*, 12650–12655.

[51] Inokuchi, D.; Hirao, Y.; Takahashi, K.; Matsumoto, K.; Mori, H.; Kubo, T. Dynamics of water molecules in a 3-fold interpenetrated hydrogen-bonded organic framework based on tetrakis(4-pyridyl)methane. *J. Phys. Chem. C* **2019**, *123*, 6599–6606.

[52] Khanpour, M.; Deng, W. Z.; Fang, Z. B.; Li, Y. L.; Yin, Q.; Zhang, A. A.; Rouhani, F.; Morsali, A.; Liu, T. F. Radiochromic hydrogen-bonded organic frameworks for X-ray detection. *Chem.—Eur. J.* **2021**, *27*, 10957–10965.

[53] Li, P. H.; Li, P.; Ryder, M. R.; Liu, Z. C.; Stern, C. L.; Farha, O. K.; Stoddart, J. F. Interpenetration isomerism in triptycene-based hydrogen-bonded organic frameworks. *Angew. Chem., Int. Ed.* **2019**, *58*, 1664–1669.

[54] Li, Y. L.; Alexandrov, E. V.; Yin, Q.; Li, L.; Fang, Z. B.; Yuan, W. B.; Proserpio, D. M.; Liu, T. F. Record complexity in the polycatenation of three porous hydrogen-bonded organic frameworks with stepwise adsorption behaviors. *J. Am. Chem. Soc.* **2020**, *142*, 7218–7224.

[55] Suzuki, Y.; Tohnai, N.; Hisaki, I. Triaxially woven hydrogen-bonded chicken wires of a tetrakis(carboxybiphenyl)ethene. *Chem.—Eur. J.* **2020**, *26*, 17056–17062.

[56] Tang, Y. C.; Zhang, C. Y.; Fan, L. L.; Shang, Y. X.; Feng, Y.; Pang, J.; Cui, X. L.; Kong, G. D.; Wang, R. M.; Kang, Z. X. et al. Regulating the orientation of hydrogen-bonded organic framework membranes based on substrate modification. *Cryst. Growth Des.* **2021**, *21*, 5292–5299.

[57] Wang, J. X.; Gu, X. W.; Lin, Y. X.; Li, B.; Qian, G. D. A novel hydrogen-bonded organic framework with highly permanent porosity for boosting ethane/ethylene separation. *ACS Mater. Lett.* **2021**, *3*, 497–503.

[58] Yang, W.; Wang, J. W.; Wang, H. L.; Bao, Z. B.; Zhao, J. C. G.; Chen, B. L. Highly interpenetrated robust microporous hydrogen-bonded organic framework for gas separation. *Cryst. Growth Des.* **2017**, *17*, 6132–6137.

[59] Yang, W.; Zhou, W.; Chen, B. L. A flexible microporous hydrogen-bonded organic framework. *Cryst. Growth Des.* **2019**, *19*, 5184–5188.

[60] Yang, Y.; Li, L. B.; Lin, R. B.; Ye, Y. X.; Yao, Z. Z.; Yang, L.; Xiang, F. H.; Chen, S. M.; Zhang, Z. J.; Xiang, S. C. et al. Ethylene/ethane separation in a stable hydrogen-bonded organic framework through a gating mechanism. *Nat. Chem.* **2021**, *13*, 933–939.

[61] Yoon, T. U.; Baek, S. B.; Kim, D.; Kim, E. J.; Lee, W. G.; Singh, B. K.; Lah, M. S.; Bae, Y. S.; Kim, K. S. Efficient separation of $C_2$ hydrocarbons in a permanently porous hydrogen-bonded organic framework. *Chem. Commun.* **2018**, *54*, 9360–9363.

[62] Zhang, X.; Wang, J. X.; Li, L. B.; Pei, J. Y.; Krishna, R.; Wu, H.; Zhou, W.; Qian, G. D.; Chen, B. L.; Li, B. A rod-packing hydrogen-bonded organic framework with suitable pore confinement for benchmark ethane/ethylene separation. *Angew. Chem., Int. Ed.* **2021**, *60*, 10304–10310.

[63] Mühlbauer, E.; Klinkebiel, A.; Beyer, O.; Auras, F.; Wuttke, S.; Lüning, U.; Bein, T. Functionalized PCN-6 metal-organic frameworks. *Microporous Mesoporous Mater.* **2015**, *216*, 51–55.

[64] Lin, Y. X.; Jiang, X. F.; Kim, S. T.; Alahakoon, S. B.; Hou, X. S.; Zhang, Z. Y.; Thompson, C. M.; Smaldone, R. A.; Ke, C. F. An elastic hydrogen-bonded cross-linked organic framework for effective iodine capture in water. *J. Am. Chem. Soc.* **2017**, *139*, 7172–7175.

[65] Karmakar, A.; Illathvalappil, R.; Anothumakkool, B.; Sen, A.; Samanta, P.; Desai, A. V.; Kurungot, S.; Ghosh, S. K. Hydrogen-bonded organic frameworks (HOFs): A new class of porous crystalline proton-conducting materials. *Angew. Chem., Int. Ed.* **2016**, *55*, 10667–10671.

[66] Qin, W. K.; Si, D. H.; Yin, Q.; Gao, X. Y.; Huang, Q. Q.; Feng, Y. N.; Xie, L.; Zhang, S.; Huang, X. S.; Liu, T. F. et al. Reticular synthesis of hydrogen-bonded organic frameworks and their derivatives via mechanochemistry. *Angew. Chem., Int. Ed.* **2022**, *61*, e202202089.

[67] Wang, L. G.; Su, H.; Zhang, Z.; Xin, J. J.; Liu, H.; Wang, X. G.; Yang, C. Y.; Liang, X.; Wang, S. W.; Liu, H. et al. Co-Co dinuclear active sites dispersed on zirconium-doped heterostructured $Co_9S_8/Co_3O_4$ for high-current-density and durable acidic oxygen evolution. *Angew. Chem., Int. Ed.* **2023**, *62*, e202314185.

[68] Samanta, J.; Dorn, R. W.; Zhang, W. L.; Jiang, X. F.; Zhang, M. S.; Staples, R. J.; Rossini, A. J.; Ke, C. F. An ultra-dynamic anion-cluster-based organic framework. *Chem* **2022**, *8*, 253–267.

[69] Wang, L. G.; Wu, J. B.; Wang, S. W.; Liu, H.; Wang, Y.; Wang, D. S. The reformation of catalyst: From a trial-and-error synthesis to rational design. *Nano Res.* **2024**, *17*, 3261–3301.

[70] Wang, L. G.; Wang, D. S.; Li, Y. D. Single-atom catalysis for carbon neutrality. *Carbon Energy* **2022**, *4*, 1021–1079.

[71] Chen, E. X.; Qiu, M.; Zhang, Y. F.; Zhu, Y. S.; Liu, L. Y.; Sun, Y. Y.; Bu, X. H.; Zhang, J.; Lin, Q. P. Acid and base resistant zirconium polyphenolate-metalloporphyrin scaffolds for efficient $CO_2$ photoreduction. *Adv. Mater.* **2018**, *30*, 1704388.

[72] Fang, Z. B.; Liu, T. T.; Liu, J. X.; Jin, S. Y.; Wu, X. P.; Gong, X. Q.; Wang, K. C.; Yin, Q.; Liu, T. F.; Cao, R. et al. Boosting interfacial charge-transfer kinetics for efficient overall $CO_2$ photoreduction via rational design of coordination spheres on metal-organic frameworks. *J. Am. Chem. Soc.* **2020**, *142*, 12515–12523.

[73] Fateeva, A.; Chater, P. A.; Ireland, C. P.; Tahir, A. A.; Khimyak, Y. Z.; Wiper, P. V.; Darwent, J. R.; Rosseinsky, M. J. A water-stable porphyrin-based metal-organic framework active for visible-light photocatalysis. *Angew. Chem., Int. Ed.* **2012**, *51*, 7440–7444.

[74] Fu, Y. H.; Sun, D. R.; Chen, Y. J.; Huang, R. K.; Ding, Z. X.; Fu, X. Z.; Li, Z. H. An amine-functionalized titanium metal-organic framework photocatalyst with visible-light-induced activity for $CO_2$ reduction. *Angew. Chem., Int. Ed.* **2012**, *51*, 3364–3367.

[75] Sun, D. R.; Fu, Y. H.; Liu, W. J.; Ye, L.; Wang, D. K.; Yang, L.; Fu, X. Z.; Li, Z. H. Studies on photocatalytic $CO_2$ reduction over $NH_2$-Uio-66(Zr) and its derivatives: Towards a better understanding of photocatalysis on metal-organic frameworks. *Chem.—Eur. J.* **2013**, *19*, 14279–14285.

[76] Xu, H. Q.; Hu, J. H.; Wang, D. K.; Li, Z. H.; Zhang, Q.; Luo, Y.; Yu, S. H.; Jiang, H. L. Visible-light photoreduction of $CO_2$ in a metal-organic framework: Boosting electron-hole separation via electron trap states. *J. Am. Chem. Soc.* **2015**, *137*, 13440–13443.

[77] Zhang, H. B.; Wei, J.; Dong, J. C.; Liu, G. G.; Shi, L.; An, P. F.; Zhao, G. X.; Kong, J. T.; Wang, X. J.; Meng, X. G. et al. Efficient visible-light-driven carbon dioxide reduction by a single-atom implanted metal-organic framework. *Angew. Chem., Int. Ed.* **2016**, *55*, 14310–14314.

[78] Yin, Q.; Alexandrov, E. V.; Si, D. H.; Huang, Q. Q.; Fang, Z. B.; Zhang, Y.; Zhang, A. A.; Qin, W. K.; Li, Y. L.; Liu, T. F. et al. Metallization-prompted robust porphyrin-based hydrogen-bonded organic frameworks for photocatalytic $CO_2$ reduction. *Angew. Chem., Int. Ed.* **2022**, *61*, e202115854.

[79] Zhang, A. A.; Li, Y. L.; Fang, Z. B.; Xie, L.; Cao, R.; Liu, Y. Y.; Liu, T. F. Facile preparation of hydrogen-bonded organic framework/$Cu_2O$ heterostructure films via electrophoretic deposition for efficient $CO_2$ photoreduction. *ACS Appl. Mater. Interfaces* **2022**, *14*, 21050–21058.

[80] Zhang, A. A.; Si, D. H.; Huang, H. B.; Xie, L.; Fang, Z. B.; Liu, T. F.; Cao, R. Partial metalation of porphyrin moieties in hydrogen-bonded organic frameworks provides enhanced $CO_2$ photoreduction activity. *Angew. Chem., Int. Ed.* **2022**, *61*, e202203955.

[81] Li, T.; Liu, B. T.; Fang, Z. B.; Yin, Q.; Wang, R.; Liu, T. F. Integrating active $C_3N_4$ moieties in hydrogen-bonded organic frameworks for efficient photocatalysis. *J. Mater. Chem. A* **2021**, *9*, 4687–4691.

[82] Mikhnenko, O. V.; Blom, P. W. M.; Nguyen, T. Q. Exciton diffusion in organic semiconductors. *Energy Environ. Sci.* **2015**, *8*, 1867–1888.

[83] Wang, H.; Liu, W. X.; He, X.; Zhang, P.; Zhang, X. D.; Xie, Y. An excitonic perspective on low-dimensional semiconductors for photocatalysis. *J. Am. Chem. Soc.* **2020**, *142*, 14007–14022.

[84] Zhou, Q. X.; Guo, Y.; Zhu, Y. F. Photocatalytic sacrificial $H_2$ evolution dominated by micropore-confined exciton transfer in hydrogen-bonded organic frameworks. *Nat. Catal.* **2023**, *6*, 574–584.

[85] Cai, J. Q.; Liu, X. M.; Gao, Z. J.; Li, L. L.; Wang, H. Chlorophylls derivatives: Photophysical properties, assemblies, nanostructures and biomedical applications. *Mater. Today* **2021**, *45*, 77–92.

[86] Kwon, N.; Kim, H.; Li, X. S.; Yoon, J. Supramolecular agents for combination of photodynamic therapy and other treatments. *Chem. Sci.* **2021**, *12*, 7248–7268.

[87] Li, X. S.; Bai, H. T.; Yang, Y. C.; Yoon, J.; Wang, S.; Zhang, X. Supramolecular antibacterial materials for combatting antibiotic resistance. *Adv. Mater.* **2019**, *31*, 1805092.

[88] Li, Z. L.; Li, S. K.; Guo, Y. H.; Yuan, C. Q.; Yan, X. H.; Schanze, K. S. Metal-free nanoassemblies of water-soluble photosensitizer and adenosine triphosphate for efficient and precise photodynamic cancer therapy. *ACS Nano.* **2021**, *15*, 4979–4988.

[89] Xie, B. R.; Li, C. X.; Yu, Y.; Zeng, J. Y.; Zhang, M. K.; Wang, X. S.; Zeng, X.; Zhang, X. Z. A singlet oxygen reservoir based on poly-pyridone and porphyrin nanoscale metal-organic framework for cancer therapy. *CCS Chem.* **2021**, *3*, 1187–1202.

[90] Yang, M. Y.; Li, X. S.; Yoon, J. Activatable supramolecular photosensitizers: Advanced design strategies. *Mater. Chem. Front.* **2021**, *5*, 1683–1693.

[91] Zou, Q. L.; Abbas, M.; Zhao, L. Y.; Li, S. K.; Shen, G. Z.; Yan, X. H. Biological photothermal nanodots based on self-assembly of peptide-porphyrin conjugates for antitumor therapy. *J. Am. Chem. Soc.* **2017**, *139*, 1921–1927.

[92] Liu, B. T.; Pan, X. H.; Nie, D. Y.; Hu, X. J.; Liu, E. P.; Liu, T. F. Ionic hydrogen-bonded organic frameworks for ion-responsive antimicrobial membranes. *Adv. Mater.* **2020**, *32*, 2005912.

[93] Wang, Y.; Cao, R.; Wang, C.; Song, X. Y.; Wang, R. N.; Liu, J. C.; Zhang, M. M.; Huang, J. Y.; You, T. T.; Zhang, Y. H. et al. *In situ* embedding hydrogen-bonded organic frameworks nanocrystals in electrospinning nanofibers for ultrastable broad-spectrum antibacterial activity. *Adv. Funct. Mater.* **2023**, *33*, 2214388.

[94] Liu, B. T.; Pan, X. H.; Zhang, D. Y.; Wang, R.; Chen, J. Y.; Fang, H. R.; Liu, T. F. Construction of function-oriented core–shell nanostructures in hydrogen-bonded organic frameworks for near-infrared-responsive bacterial inhibition. *Angew. Chem., Int. Ed.* **2021**, *60*, 25701–25707.

[95] Lee, S. K.; Zu, Y. B.; Herrmann, A.; Geerts, Y.; Müllen, K.; Bard, A. J. Electrochemistry, spectroscopy and electrogenerated chemiluminescence of perylene, terrylene, and quaterrylene diimides in aprotic solution. *J. Am. Chem. Soc.* **1999**, *121*, 3513–3520.

[96] Yang, Y. C.; He, P.; Wang, Y. X.; Bai, H. T.; Wang, S.; Xu, J. F.; Zhang, X. Supramolecular radical anions triggered by bacteria *in situ* for selective photothermal therapy. *Angew. Chem., Int. Ed.* **2017**, *56*, 16239–16242.

[97] Zhang, A. D.; Jiang, W.; Wang, Z. H. Fulvalene-embedded perylene diimide and its stable radical anion. *Angew. Chem., Int. Ed.* **2020**, *59*, 752–757.

[98] Yang, J.; Choi, J.; Bang, D.; Kim, E.; Lim, E. K.; Park, H.; Suh, J. S.; Lee, K.; Yoo, K. H.; Kim, E. K. et al. Convertible organic nanoparticles for near-infrared photothermal ablation of cancer cells. *Angew. Chem., Int. Ed.* **2011**, *50*, 441–444.

[99] Zhou, B.; Yan, D. P. Hydrogen-bonded two-component ionic crystals showing enhanced long-lived room-temperature phosphorescence via TADF-assisted förster resonance energy transfer. *Adv. Funct. Mater.* **2018**, *29*, 1807599.

[100] Yin, W. Y.; Yu, J.; Lv, F. T.; Yan, L.; Zheng, L. R.; Gu, Z. J.; Zhao, Y. L. Functionalized nano-$MoS_2$ with peroxidase catalytic

and near-infrared photothermal activities for safe and synergetic wound antibacterial applications. *ACS Nano* **2016**, *10*, 11000–11011.

[101] Liang, W. B.; Carraro, F.; Solomon, M. B.; Bell, S. G.; Amenitsch, H.; Sumby, C. J.; White, N. G.; Falcaro, P.; Doonan, C. J. Enzyme encapsulation in a porous hydrogen-bonded organic framework. *J. Am. Chem. Soc.* **2019**, *141*, 14298–14305.

[102] Yu, D. Q.; Zhang, H. C.; Liu, Z. Q.; Liu, C.; Du, X. B.; Ren, J. S.; Qu, X. G. Hydrogen-bonded organic framework (HOF)-based single-neural stem cell encapsulation and transplantation to remodel impaired neural networks. *Angew. Chem., Int. Ed.* **2022**, *61*, e202201485.

[103] Björn, L. O. Photoenzymes and related topics: An update. *Photochem. Photobiol.* **2018**, *94*, 459–465.

[104] Li, W. P.; Shi, J. F.; Chen, Y.; Liu, X. Y.; Meng, X. X.; Guo, Z. Y.; Li, S. H.; Zhang, B. Y.; Jiang, Z. Y. Nano-sized mesoporous hydrogen-bonded organic frameworks for *in situ* enzyme immobilization. *Chem. Eng. J.* **2023**, *468*, 143609.

[105] Tong, L. J.; Lin, Y. H.; Kou, X. X.; Shen, Y. J.; Shen, Y.; Huang, S. M.; Zhu, F.; Chen, G. S.; Ouyang, G. F. Pore-environment-dependent photoresponsive oxidase-like activity in hydrogen-bonded organic frameworks. *Angew. Chem., Int. Ed.* **2023**, *62*, e202218661.

[106] He, Z.; Li, Y. Q.; Wu, H.; Yang, Y. H.; Chen, Y. L.; Zhu, J. K.; Li, Q. N.; Jiang, G. H. Novel stimuli-responsive spiropyran-based switch@HOFs materials enable dynamic anticounterfeiting. *ACS Appl. Mater. Interfaces* **2022**, *14*, 48133–48142.

[107] Liu, B. T.; Liu, E. P.; Sa, R. J.; Liu, T. F. Crystalline hydrogen-bonded organic chains achieving ultralong phosphorescence via triplet-triplet energy transfer. *Adv. Opt. Mater.* **2020**, *8*, 2000281.

[108] Paulsen, B. D.; Tybrandt, K.; Stavrinidou, E.; Rivnay, J. Organic mixed ionic-electronic conductors. *Nat. Mater.* **2020**, *19*, 13–26.

[109] Chen, S. M.; Ju, Y.; Zhang, H.; Zou, Y. B.; Lin, S.; Li, Y. B.; Wang, S. Q.; Ma, E.; Deng, W. H.; Xiang, S. C. et al. Photo responsive electron and proton conductivity within a hydrogen-bonded organic framework. *Angew. Chem., Int. Ed.* **2023**, *62*, e202308418.

[110] Huang, Q. Y.; Chen, X. X.; Li, W. L.; Yang, Z. Y.; Zhang, Y.; Zhao, J.; Chi, Z. G. Local dynamics in a hydrogen-bonded organic framework for adaptive guest accommodation with programmable luminescence. *Chem* **2023**, *9*, 1241–1254.

[111] Han, B.; Wang, H. L.; Wang, C. M.; Wu, H.; Zhou, W.; Chen, B. L.; Jiang, J. Z. Postsynthetic metalation of a robust hydrogen-bonded organic framework for heterogeneous catalysis. *J. Am. Chem. Soc.* **2019**, *141*, 8737–8740.

[112] Lin, R. B.; He, Y. B.; Li, P.; Wang, H. L.; Zhou, W.; Chen, B. L. Multifunctional porous hydrogen-bonded organic framework materials. *Chem. Soc. Rev.* **2019**, *48*, 1362–1389.

[113] Yu, B. Q.; Li, L. J.; Liu, S. S.; Wang, H. L.; Liu, H. Y.; Lin, C. X.; Liu, C.; Wu, H.; Zhou, W.; Li, X. Y. et al. Robust biological hydrogen-bonded organic framework with post-functionalized rhenium(I) sites for efficient heterogeneous visible-light-driven $CO_2$ reduction. *Angew. Chem., Int. Ed.* **2021**, *60*, 8983–8989.

[114] Huang, Q. Y.; Li, W. L.; Mao, Z.; Qu, L. J.; Li, Y.; Zhang, H.; Yu, T.; Yang, Z. Y.; Zhao, J.; Zhang, Y. et al. An exceptionally flexible hydrogen-bonded organic framework with large-scale void regulation and adaptive guest accommodation abilities. *Nat. Commun.* **2019**, *10*, 3074.

[115] Horike, S.; Shimomura, S.; Kitagawa, S. Soft porous crystals. *Nat. Chem.* **2009**, *1*, 695–704.

[116] Huang, Q. Y.; Li, W. L.; Mao, Z.; Zhang, H.; Li, Y.; Ma, D. Y.; Wu, H. Y.; Zhao, J.; Yang, Z. Y.; Zhang, Y. et al. Dynamic molecular weaving in a two-dimensional hydrogen-bonded organic framework. *Chem* **2021**, *7*, 1321–1332.

[117] Xiao, W. C.; Hu, C. H.; Ward, M. D. Guest exchange through single crystal-single crystal transformations in a flexible hydrogen-bonded framework. *J. Am. Chem. Soc.* **2014**, *136*, 14200–14206.

[118] Huang, Y. G.; Shiota, Y.; Wu, M. Y.; Su, S. Q.; Yao, Z. S.; Kang, S.; Kanegawa, S.; Li, G. L.; Wu, S. Q.; Kamachi, T. et al. Superior thermoelasticity and shape-memory nanopores in a porous supramolecular organic framework. *Nat. Commun.* **2016**, *7*, 11564.

[119] Lv, Y. C.; Liang, J. S.; Xiong, Z. L.; Yang, X.; Li, Y. B.; Zhang, H.; Xiang, S. C.; Chen, B. L.; Zhang, Z. J. Smart-responsive HOF heterostructures with multiple spatial-resolved emission modes toward photonic security platform. *Adv. Mater.* **2024**, *36*, 2309130.

[120] Xu, X.; Yan, B. Bioinspired luminescent HOF-based foam as ultrafast and ultrasensitive pressure and acoustic bimodal sensor for human-machine interactive object and information recognition. *Adv. Mater.* **2023**, *35*, 2303410.

[121] Hisaki, I.; Suzuki, Y.; Gomez, E.; Ji, Q.; Tohnai, N.; Nakamura, T.; Douhal, A. Acid responsive hydrogen-bonded organic frameworks. *J. Am. Chem. Soc.* **2019**, *141*, 2111–2121.

[122] Wang, Y.; Zheng, X. B.; Wang, D. S. Design concept for electrocatalysts. *Nano Res.* **2021**, *15*, 1730–1752.

[123] Wu, Y. L.; Mao, X. N.; Zhang, M. C.; Zhao, X.; Xue, R. J.; Di, S. J.; Huang, W.; Wang, L.; Li, Y. Y.; Li, Y. G. 2D molecular sheets of hydrogen-bonded organic frameworks for ultrastable sodium-ion storage. *Adv. Mater.* **2021**, *33*, 2106079.

[124] Zhao, X.; Yin, Q.; Mao, X. N.; Cheng, C.; Zhang, L.; Wang, L.; Liu, T. F.; Li, Y. Y.; Li, Y. G. Theory-guided design of hydrogen-bonded cobaltoporphyrin frameworks for highly selective electrochemical $H_2O_2$ production in acid. *Nat. Commun.* **2022**, *13*, 2721.

[125] Hao, Q.; Li, Z. J.; Lu, C.; Sun, B.; Zhong, Y. W.; Wan, L. J.; Wang, D. Oriented two-dimensional covalent organic framework films for near-infrared electrochromic application. *J. Am. Chem. Soc.* **2019**, *141*, 19831–19838.

[126] Kung, C. W.; Wang, T. C.; Mondloch, J. E.; Fairen-Jimenez, D.; Gardner, D. M.; Bury, W.; Klingsporn, J. M.; Barnes, J. C.; Van Duyne, R.; Stoddart, J. F. et al. Metal-organic framework thin films composed of free-standing acicular nanorods exhibiting reversible electrochromism. *Chem. Mater.* **2013**, *25*, 5012–5017.

[127] Stec, G. J.; Lauchner, A.; Cui, Y.; Nordlander, P.; Halas, N. J. Multicolor electrochromic devices based on molecular plasmonics. *ACS Nano.* **2017**, *11*, 3254–3261.

[128] Matsui, J.; Kikuchi, R.; Miyashita, T. A trilayer film approach to multicolor electrochromism. *J. Am. Chem. Soc.* **2014**, *136*, 842–845.

[129] Woodward, A. N.; Kolesar, J. M.; Hall, S. R.; Saleh, N. A.; Jones, D. S.; Walter, M. G. Thiazolothiazole fluorophores exhibiting strong fluorescence and viologen-like reversible electrochromism. *J. Am. Chem. Soc.* **2017**, *139*, 8467–8473.

[130] Takada, K.; Sakamoto, R.; Yi, S. T.; Katagiri, S.; Kambe, T.; Nishihara, H. Electrochromic bis(terpyridine)metal complex nanosheets. *J. Am. Chem. Soc.* **2015**, *137*, 4681–4689.

[131] Feng, J. F.; Liu, T. F.; Cao, R. An electrochromic hydrogen-bonded organic framework film. *Angew. Chem., Int. Ed.* **2020**, *59*, 22392–22396.

[132] Feng, J. F.; Luo, Y.; Wang, X. Y.; Cai, G. F.; Cao, R. A large-area patterned hydrogen-bonded organic framework electrochromic film and device. *Small* **2023**, *19*, 2304691.

[133] Gao, X. Y.; Lu, W. Y.; Wang, Y.; Song, X. Y.; Wang, C.; Kirlikovali, K. O.; Li, P. Recent advancements of photo- and electro-active hydrogen-bonded organic frameworks. *Sci. China Chem.* **2022**, *65*, 2077–2095.

[134] Lu, M. L.; Huang, W.; Gao, S. Z.; Zhang, J. L.; Liang, W. B.; Li, Y.; Yuan, R.; Xiao, D. R. Pyrene-based hydrogen-bonded organic frameworks as new emitters with porosity- and aggregation-induced enhanced electrochemiluminescence for ultrasensitive MicroRNA assay. *Anal. Chem.* **2022**, *94*, 15832–15838.

[135] Wang, C.; Wang, Y.; Kirlikovali, K. O.; Ma, K. K.; Zhou, Y. M.; Li, P.; Farha, O. K. Ultrafine silver nanoparticle encapsulated porous molecular traps for discriminative photoelectrochemical detection of mustard gas simulants by synergistic size-exclusion and site-specific recognition. *Adv. Mater.* **2022**, *34*, 2202287.

[136] Wang, C.; Song, X. Y.; Wang, Y.; Xu, R.; Gao, X. Y.; Shang, C.; Lei, P.; Zeng, Q. D.; Zhou, Y. M.; Chen, B. L. et al. A solution-processable porphyrin-based hydrogen-bonded organic framework for photoelectrochemical sensing of carbon dioxide. *Angew. Chem., Int. Ed.* **2023**, *62*, e202311482.